



LIBRARY
Michigan State
University

This is to certify that the thesis entitled

NONLINEAR DYNAMICS OF LOW IMMERSION MACHINING

presented by

Ming Liao

has been accepted towards fulfillment of the requirements for

MS Mechanical Engineering degree in _____

Major professor

Date 8/23/00

MSU is an Affirmative Action/Equal Opportunity Institution

O-7639

PLACE IN RETURN BOX to remove this checkout from your record.

TO AVOID FINES return on or before date due.

MAY BE RECALLED with earlier due date if requested.

DATE DUE	DATE DUE	DATE DUE

11/00 c:/CIRC/DateDue.p85-p.14

NONLINEAR DYNAMICS OF LOW IMMERSION MACHINING

Ву

Ming Liao

A THESIS

Submitted to
Michigan State University
In partial fulfillment of the requirements
For the Degree of

MASTER OF SCIENCE

Department of Mechanical Engineering

2000

ABSTRACT

NONLINEAR DYNAMICS OF LOW IMMERSION MACHINING

By

Ming Liao

A nonlinear theory of chatter in interrupted machining is developed. The machine tool structure is represented by an equivalent single degree of freedom system with nonlinear cutting force which obeys a digressive function (α) of chip thickness. For highly interrupted machining processes, the system is simplified to an impact model with the nonlinear time delay term. An approximate analytic solution of the system is obtained from this model and the stability charts of the machining operations are estimated analytically. Unlike the continuous cutting, the number of stability lobes is doubled. For certain cutting conditions, the Hopf bifurcation and period-doubling bifurcation occurs alternatively with the increase of spindle speed. Both Hopf bifurcations and perioddoubling bifurcations are subcritical as $0<\alpha<1$. An additional nonlinearity is introduced by the vibrating tool leaving the workpiece frequently after the bifurcation occurs. The global bifurcations are predicted and verified by numerical simulations. Although the results are demonstrated using an interrupted turning example, it is anticipated that the theory will be most useful for high-speed, finish-milling operations where the radialdepth-of-cut is only a small fraction of the tool diameter.

To my family

ACKNOWLEDGEMENTS

I would like to express my deepest appreciation to the following people and institutes for having made the completion of this thesis possible.

To the National Science Foundation for funding some related research which let to the research in this thesis (NSF, grant No. DMI-9800323).

To my advisor Dr. Brian Feeny, for his guidance and invaluable assistance, without which this thesis would not have been possible.

To Dr. Matt Davis, National Institute of Standards and Technology (NIST), on the basis of whose work this paper was begun to be developed in the summer of 1999. His dedications to the subject and personal integrity have served as an example and an inspiration to me.

To my other committee members, Dr. Steve Shaw and Dr. Dinesh Balabangadhar, for their kind help and useful advice.

To Dr. Jon Pratt, and Dr. Tim Burns, NIST, for the fruitful discussions we had.

To all my other instructors and colleagues at MSU, for their skillful instructions in the classroom and lab, but more importantly, for their friendship and constant encouragement.

To my family, for years of support, patience and understanding.

TABLE OF CONTENTS

LIST OF FIGURES	vi
KEY TO SYMBOLS OR ABBREVIATIONS	viii
CHAPTER 1	
INTRODUCTION	1
1.1 Machine Dynamics	1
1.2 Low Immersion Milling	
1.3 Nonlinear Dynamics of Machining	12
1.6 Contributions	
CHAPTER 2	
THEORETICAL ANALYSIS	
2.1 Modeling of the Interrupt Cutting	
2.1.1 Basic Assumptions	
2.1.2 Modeling of Interrupted Turning	
2.1.3 Modeling of Low Immersion Milling	
2.2 Approximate Analytic Solution	
2.3 Local Stability	
2.4 Local Bifurcations	38
2.5 The Role of α	46
2.6 Post Bifurcation Orbits	53
CHAPTER 3	
SIMULATIONS AND EXPERIMENTS	
3.1 Simulations	
3.2 Experiments	75
CHAPTER 4	
CONCLUSIONS AND SUGGESTIONS FOR FUTURE WORK	77
RIRI IOGRAPHY	80

LIST OF FIGURES

1.1	Regeneration in turning	2
1.2	Stability chart for a turning operation	6
1.3	Sketch of Low Immersion Milling	9
1.4	Stability curve for uninterrupted and highly interrupted turning operations	11
2.1	Schematic of an interrupted turning operation	19
2.2	Schematic of a low immersion milling operation	19
2.3	The relation between cutting force and chip thickness	21
2.4	Cutting force series in interrupted machining	27
2.5	The ways the eigenvalues travel through the unit circle	33
2.6	Stability lobes diagram of interrupted turning	35
2.7	Parameter traces for bifurcations	39
2.8	Subcritical period-doubling bifurcation diagram	42
2.9	Subcritical Hopf bifurcation diagram	46
2.10	The comparison of stability charts from the nonlinear model and the linear	
	model	48
2.11	Period-doubling bifurcation diagrams at different values of α	50
2.12	Hopf bifurcation diagrams at different values of α	52
2.13	Hopf bifurcation diagram in continuous cutting	55
2.14	Global bifurcation diagram for period-doubling bifurcation case	59

2.15	Possible ways that chatter amplitude stabilizes at the cut-no-cut period-two orb	it
		60
2.16	Global bifurcation diagram for Hopf bifurcation case	63
2.17	Possible ways that chatter amplitude becomes quasiperiodic	.64
3.1	Comparison of stability lobes obtained from analytic solutions and from	
	simulations	.69
3.2	Stable period-two orbit after the subcitical period-doubling bifurcation	.71
3.3	Quasiperiodic orbit after the subcitical Hopf bifurcation	.71
3.4	Comparison of in-cut passes and out-of-cut passes for quasiperiodic orbits	72
3.5	Simulations of the subcritical period-doubling bifurcation diagram	74
3.6	Simulations of the subcritical Hopf bifurcation diagram	.74
3.7	Comparison of stability charts from experiments of 5% immersion and 25%	
	immersion end-milling	76
3.8	Comparison of stability charts from analytical prediction and experiments	
	of 5% immersion end-milling	.76

KEY TO SYMBOLS OR ABBREVIATIONS

SYMBOL	MEANING	UNITS
m	Equivalent mass of the system	kg
c	Damping coefficient of equivalent dashpot	N.s/m
k	Stiffness coefficient of equivalent spring	N/m
K_t	Thrust force coefficient	N/m ²
w	Axial depth of chip	m
d	Radial depth of chip	m
T	Tool engagement period	S
Ω	Spindle speed	1/s
τ	transition time for free vibrations	s
N	The number of flutes on the end-mill	
N fo		flute or m/rev
		flute or m/rev
fo	Feed rate m/	flute or m/rev rad/s
fo ζ	Feed rate m/ Damping ratio	
fo ζ ω_n	Feed rate m/ Damping ratio Natural frequency of the system	rad/s
fo ζ ω_n	Feed rate m/ Damping ratio Natural frequency of the system Damped frequency of the system	rad/s rad/s
f_0 ζ ω_n ω_d	Feed rate m/ Damping ratio Natural frequency of the system Damped frequency of the system Natural frequency of the system	rad/s rad/s Hz
f_0 ζ ω_n ω_d f_n	Feed rate m/ Damping ratio Natural frequency of the system Damped frequency of the system Natural frequency of the system Damped frequency of the system	rad/s rad/s Hz

CHAPTER 1

INTRODUCTION

Section 1.1: Machine Dynamics

In machine dynamics, one big issue is the conditions of the occurrence of the selfexcited vibrations called "chatter".

Chatter is caused mainly by "regeneration of waviness" on the machined surface. Regeneration is possible because in almost all machining operations the tool removes the chip from a surface which was produced by the tool in the preceding pass, i.e., the surface produced in tuning during the preceding revolution or, in milling, by the preceding tooth of the cutter.

For example, in turning operations, if there is relative vibration between tool and workpiece, waviness is generated on the cut surface. The tool in the next revolution encounters a wavy surface and removes a chip with periodically variable thickness. The cutting force is then periodically variable. This produces vibrations, and depending on conditions derived later, these vibrations may be at least as large as in the preceding revolution. The newly created surface is again wavy, and in this way, the waviness is continually regenerated. In a "stable" case any initial vibration diminishes in subsequent passes; in an "unstable" case it increases, and at the "limit of stability" the magnitude of the vibration remains constant. Figure 1.1 shows the regeneration in turning operations.

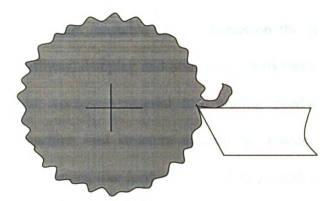


Figure 1.1 regeneration in turning

Milling is a much more complex case than turning as regards chatter generation. In milling, the "subsequent passes" are represented by the cuts of the individual teeth of the cutter, each of them regenerating the waviness created by the preceding tooth. So the phasing between those subsequent undulations is not determined by the number of waves per revolution as in turning, but by the waves per tooth spacing. It means, basically, for the same spindle speed, the number of waves between teeth may be small, or even to zero.

When chatter occurs, the machined surface is spoiled by chatter marks. Vibrations can be so strong that the tool may leave the workpiece, i.e., the amplitude of the vibration between tool and workpiece becomes larger than the chip thickness. Cutting force can oscillate with peaks of at least double the mean value. These vibrations, especially in machining stronger materials, might lead to the breakage of tools. This aspect as well as the aspect of surface finish requires that machining parameters be kept in a region for which the chatter does not occur. This generally limits the material removal rate. In aircraft manufacture, i.e., mostly in end milling of aluminum, chatter is unavoidable and

many hours of labor are spent on manually removing chatter marks which would otherwise decrease the fatigue life of the machined parts.

Whether or not chatter occurs (unstable case) depends on the structure of the machine and workpiece, the stiffness, damping and orientation of its modes of vibration, and on the conditions of the cut: workpiece material, feed, cutting speed and chip width. For a given operation, the machine tool structure and the workpiece are not freely selectable, while the cutting parameters, like feed, speed, and chip width, are tunable for an optimal productivity. It is recognized that the most significant cutting parameter which is decisive for the generation of chatter is the width of cut (chip width) (Tlusty, 1993), denoted as w. For sufficiently small chip widths cutting is stable, without chatter. By increasing chip width w, chatter starts to occur at a certain value—limit chip width, denoted as w_{lim} , and becomes more energetic for all values of $w > w_{lim}$. The value of w_{lim} depends on the dynamic characteristics of the structure, on the workpiece material, on the cutting speed and feed, and on the geometry of the tool.

Extensive research has been devoted to the problems of chatter in machining. Arnold (1946) first suggested regeneration of waves on the workpiece as a potential cause of chatter. Tobias and Fishwick (1958), Tlusty and Polacek (1957, 1963) and Merrit (1965) did notable experimental and analytical efforts. They built mathematical models of machining and represented the stability regions in the form of stability charts. Following these pioneering efforts, there have been many efforts to understand regenerative stability in machining operations.

Shridar (1968) developed a mathematical model for general milling processes. In his paper, a more complete description of the milling process is formulated. The resulting

equation is a general *n*th order vector-matrix linear equation with periodic coefficients and a transport lag. Or equally, it is a set of linear first-order differential equations (state variable form), convenient for stability analysis. He concluded that the chatter analysis was associated with the stability characteristics of linear differential equations with periodic coefficients and it did not appear that stability methods based on frequency analysis can be used to study chatter in a milling operation.

Shridar (1968) also gave a stability algorithm for the general milling process. The algorithm can be used in conjunction with the digital computer and developed as a means of analytically determining the stability of the linear differential equation. The algorithm permitted the dtermination of the stability boundaries in the space of controllable parameters associated with a cutting operation.

Tlusty, Ismail, Zaton and Smith (1981, 1983, 1986,1991) studied milling stability by means of time domain simulations. They showed that high gains of stability are achievable by determining and using a particular spindle speed such that the cutter tooth frequency approaches the frequency of the decisive mode of vibrations as measured on the cutter. Specifically, they made the following conclusions on high speed milling: the process damping which stabilizes cutting at conventional speeds is absent in high-speed milling; high-speed, high-power face milling and short end milling can only be stable if the rigidity of high-speed spindles is substantially increased; that high-speed milling with long end mills is much more difficult from the point of view of chatter because of the inherent low stiffness of the tool itself. They also pointed out the influence the possibility of interactions between regenerative vibrations and vibrations induced by the intermittent

engagement of the tool and workpiece. However, the possibility that the intermittency itself could lead to vibration instability was not discussed.

Altintas and Budak (1995) produced analytical stability lobes in the milling operation. The stability model required transfer functions of the structure at the cutterworkpiece contact zone, static cutting force coefficients, radial immersion and the number of teeth on the cutter. Time varying dynamic cutting force coefficients were approximated by their Fourier series components, and the chatter free axial depth of cuts and spindle speeds were calculated directly from the proposed set of linear analytic expressions without any digital iteration. The result was in excellent agreement with the time domain simulations and multi-frequency solutions

Recently, there have been more researchers working on the problem of chatter. Many methods have been proposed to prevent chatter in machining. Typically, three approaches are preferred. The first is to design and set up the right kind of machine tool structure which leads to improved stability. The second is to choose optimal spindle speeds, and the third is to design and manufacture milling cutters with non-uniform tooth pitch and with alternating helix as well as with serrated or undulated edges.

In a machining system, the machine tool structure and tool geometry are already given. It is more feasible to choose the optimal speeds to increase the stability and productivity. Fortunately, at the limit of stability, the width of cut and the spindle speed have a relationship such as that shown in the stability chart of Figure 1.2. The stability lobes shown here mark the boundary between stable and unstable cuts of operation, the area below the lobes representing stable operation zones and the area above, unstable operating zones. It can be seen from the figure that at some optimal speeds, the limit chip

width can be much larger than the others, and the higher the spindle speed, the larger the limit chip width. So, by increasing the spindle speed, not only the productivity is increased, but the stability is also improved. This is what makes the high-speed machining more and more prosperous.

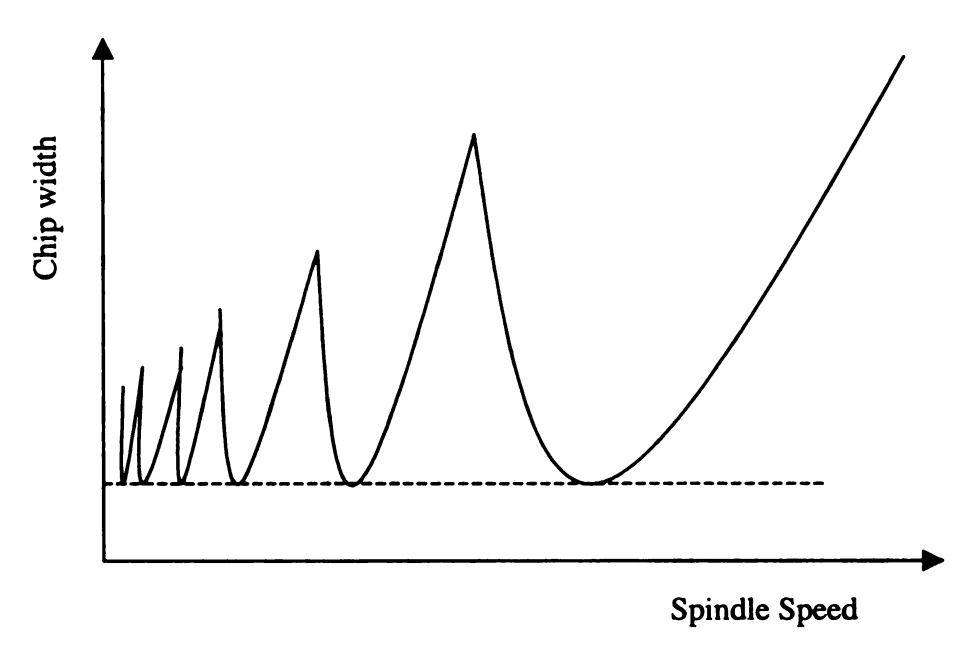


Figure 1.2 Stability chart for a continuous cutting operation (above the stability lobes are chatter regions; below are stable regions.)

Most recently, high-speed machining technology has been rapidly commercialized in industry. Researchers found that the high-speed machining has never been so important in industries until today. In less than 20 years, the spindle speeds, feed rates and power capabilities of production-grade machining centers have increased by more than a factor of ten. Currently, commercially available machining centers can be obtained with spindles capable of speeds exceeding 40 thousand revolutions per minute (krpm) while delivering 40 kW of continuous power to the cutting zone, and slides capable of producing linear motions at speeds and accelerations exceeding 1 m/s and 10 m/s², respectively (Davies et al., 1999a).

In the aerospace and automotive industries, the high-speed machining technology has been applied widely, especially in manufacture of aluminum components where volumetric material removal rates can be extremely high, often approaching thousands of cubic centimeters per minute. The advantages of high-speed machining include:

- (1) shorter machining time;
- (2) improved surface finish;
- (3) reduced thermal and mechanical stresses on the workpiece and tool; and
- (4) improved dynamic stability.

Halley and Helvey (1999) at Boeing, and Tlusty, Smith, and Ismail (1991, 1996) at University of Florida, did a lot of research on high-speed machining on the manufacture of aluminum components, the results are very encouraging. But progress in high-speed machining of other materials has been more limited except some special examples.

Of many factors which affect the material removal rate in high-speed machining, two primary limitations are:

- (1) tool wear; and
- (2) dynamical stability.

In high-speed machining aluminum components, with tungsten carbide cutting tool, the tool wear rates can be ignored. The primary limitation is dynamic stability. Fortunately, as predicted in Figure 1.2, in the high-speed region, the chatter lobes are much less densely packed, and the limit chip width is dramatically increased at the optimal spindle speeds. This means increasing the spindle speed can improve the dynamical stability.

Unfortunately, in high-speed machining more difficult materials, the tool wear can no longer be ignored. High temperature caused by high-speed machining and high material removal rates can lead to rapid catastrophic tool failure. To reduce the tool wear, there is a tendency to decrease the cutting speed. For high-speed machining materials that cause non-negligible tool wear, a compromise must be struck between reduced wear rates and improved stability. This is not a preferred choice. One alternative strategy is to use the low immersion machining.

Section 1.2 Low Immersion Machining

According to Davies et al. (1999a), low immersion machining means that the radial depth-of-cut is very low so that the partial immersion ratio ρ (defined as the ratio of time spent in cutting to not in cutting) is very small, sometimes as low as a few percent. Low immersion is often used in high-speed machining, especially in high-speed milling. In Figure 1.3, the schematics show the comparison between low immersion machining and deep immersion machining.

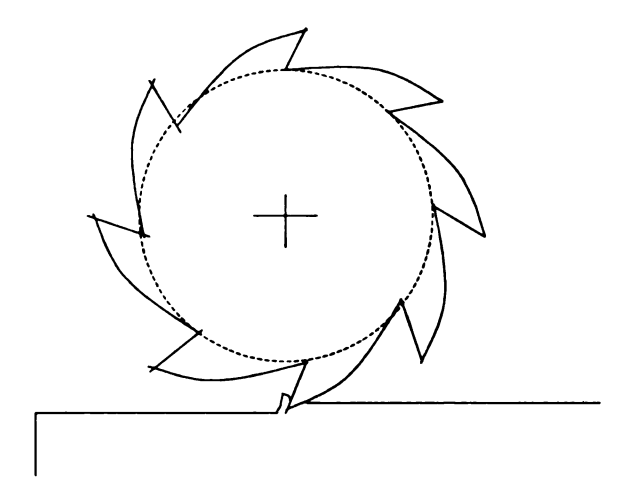


Figure 1.3 (a) Sketch of Low Immersion Milling

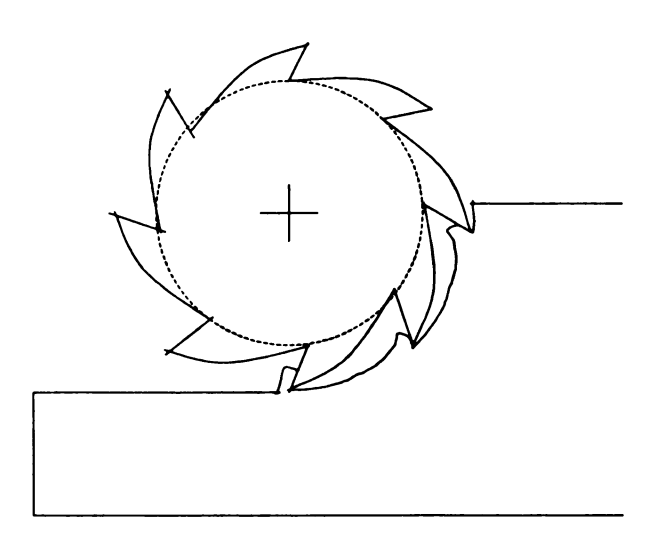


Figure 1.3(b) Sketch of Deep Immersion milling

The low immersion machining has the following advantages.

(1) Reducing the tool wear. The reason for this is that during the portion of the time when the tool is not cutting, the water (coolant) runs directly on those portions of the lip surface and cutting edge of the tool which do the work. For

- this reason the tool is more effectively cooled with intermittent work than with steady work (Taylor, 1907).
- (2) Increasing the stability. First, a rather higher cutting speed can be used with an intermittent cut than with a steady one because of the reduced tool wear. Second, with highly interrupted cutting, the tool has more time in damping to overcome the oscillating energy obtained from cutting.
- (3) **Better surface finish**. This is straightforward and is especially suitable for sculpted surfaces.
- (4) Suitable for near-net-shape workpieces. With the development of manufacture technologies, the near-net-shape workpieces are more and more widely used to reduce the total amount of material that must be removed by machining.

With reduced tool wear and increased stability, the spindle speed can be very high. The limit chip width could be significantly increased at the optimal spindle speeds. The loss of material removal rates caused by reduced radial depths of cut can be compensated by increased axial depths of cut. Overall this could produce substantial improvements in the attainable material removal rates. Recently, Smith et al. (1999) did some investigations on the effect of reduced radial immersion on high-speed machining of titanium alloys, with encouraging results.

The major feature of low immersion machining is the highly interrupted cutting. The dynamics of low immersion machining is dramatically different from the deep immersion machining or continuous cutting because the intermittent cut introduces an impact-type nonlinearity. Each of the stability lobes in continuous cutting is split into two

lobes because of the impact induced dynamics, as shown in Figure 1.4. The total number of stability lobes of interrupted cutting is doubled compared to continuous cutting. The newly found stable regions in stability chart is doubled compared to continuous cutting. The conventional model based on the continuous cutting is no longer valid to predict the stability for interrupted machining.

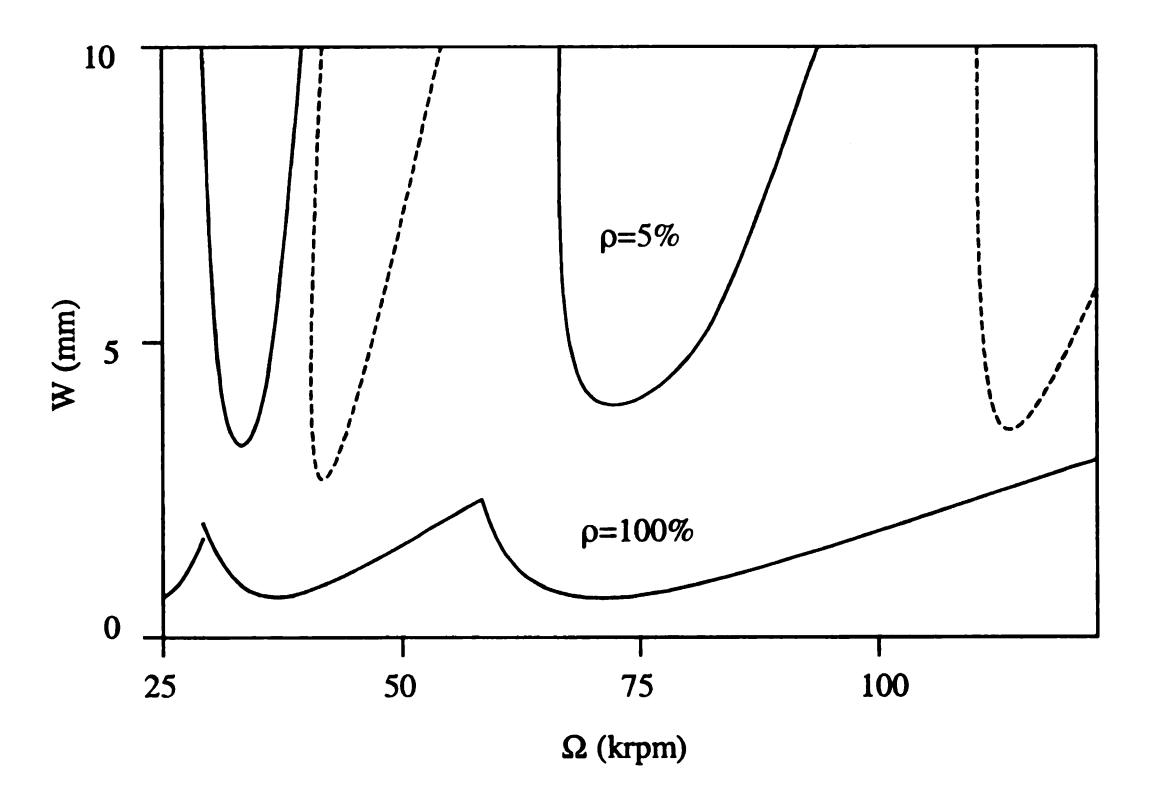


Figure 1.4 Simulated stability lobes for uninterrupted and highly interrupted turning operations. (ρ =5%: highly interrupted turning; ρ =100%: uninterrupted turning; parameters: k=1.4MN/m, m=0.043kg, c=8.6N-s/m) Courtesy of M. A. Davies.

Davies et al. (1999a) developed a linear theory for the interrupted machining. Using two examples, interrupted turning and low immersion end-milling, he built a linear model for interrupted machining. The machine tool structure was represented with a single-degree-of-freedom system with a linear delayed term. The system then was treated

as a two-stage map. For the first stage, the tool was not in contact with the workpiece. The system was just in free vibration and the solution was straightforward. For the second stage, the tool was engaging in cut. There was no general analytic, time-domain solution for this stage, instead, an approximate analytic solution was sought. With the assumption of a very small immersion ratio, the time of contact was very short compared to the characteristic period of vibration for the system. The result of the cutting action was to provide an impulsive change in the momentum of the oscillating body, and the system reduced to a kicked harmonic oscillator with delay (Zaslavsky et al. (1978, 1991)). The kicked-oscillator produced a simple map. The stability was analytically determined. This linear theory predicted the doubling in the number of stability lobes. This had significant meaning for the determination of the optimal cutting conditions for low-radial immersion high-speed machining.

However, because of high spindle speeds and high-slide accelerations, maintaining accuracy in high-speed machining requires the development of more accurate dynamic models of the machine and cutting process. Linear models are inadequate to obtain the enough accuracy and they are also incompetent for explain many nonlinearities in machining. Nonlinear models are often required where linear models fail.

Section 1.3 Nonlinear Dynamics of Machining

According to the linear theory of chatter, the amplitude of vibration ought to increase indefinitely once the width of cut exceeds a certain critical value and the process

becomes unstable. This is not so in practice when the amplitude, after a rapid initial increase stabilizes itself at a finite level. This stabilization phenomenon is explained by most investigators as being due to nonlinearities in the system.

An exploration of nonlinear region of chatter is of importance also from the point of view of correlating experimental and theoretical results. The linear theory predicts the threshold of stability in the form of a stability chart. In actual experiments such threshold conditions cannot be set up and the chatter vibration actually investigated is already stabilized by nonlinear effects. As a result, experimentally determined stability charts may differ considerably from those predicted theoretically.

The linear theory is inadequate also for explain "finite amplitude instability" (Tobias(1974)). Systems which show this effect have the characteristics of being stable for small disturbances but unstable when these become sufficiently large, as may arise in intermittent cutting.

Probably Hanna and Tobias (1974) are the earliest researchers who investigated the nonlinearities in chatter analysis. They represented the machine-tool structure by a single-degree-of-freedom system with nonlinear stiffness characteristics and modeled the cutting force as a third degree polynomial of the chip thickness. This model led to a second-order differential equation with nonlinear stiffness and nonlinear time-delay terms that was analyzed using a two-term harmonic balance.

Shi and Tobias (1984) improved this model by showing that "finite amplitude instability" could be understood without assuming a non-linear behavior of the machine tool structure; it was due to the regenerative conditions arising when the tool left the

workpiece material and the nonlinearity of the cutting force as a function of the chip thickness.

In contrast, Tlusty and Ismail (1982) turned to numerics to characterize the nonlinearity associated with the tool leaving the workpiece. They developed a time-domain simulation using a two-degree-of-freedom model of the machine-tool structure. The cutting force is assumed to be proportional to the chip thickness when the tool is cutting and zero whenever the tool vibrates out of the cut. In addition, the chip thickness at any time t depends on the tool displacements at previous times *t-T*, *t-2T*, *t-3T*, etc. This dependence is referred to as "multiple regenerative" effect.

Grabec (1986, 1988) used a linear two-degree-of-freedom model from machine-tool structure and coupled the two degrees of freedom through a friction coefficient. He did not consider regeneration. The cutting force was modeled as a quadratic function of the chip thickness and velocity and was derived from the experimental results reported by Hastings et al. (1971, 1980) for stable cutting. Grabec numerically integrated the equations of motion and found that the vibration undergoes a bifurcation from quasiperiodic to chaotic as the mean cutting force was increased.

Lin and Weng (1990) used a single-degree-of-freedom model with regeneration and non-linear dependence on chip thickness and velocity to investigate the nonlinear stability limit. They used the method of multiple scales to determine analytically a limit width of cut for orthogonal cutting. They have also considered a two-degree-of-freedom model with the addition of multiple regeneration (Lin and Weng, 1991). This study was numerical and demonstrated chaotic dynamics.

A single-degree-of-freedom modal incorporating time-delay effects and nonlinear velocity-dependent friction force at the tool/workpiece interface was investigated by Moon (1994). He suggested that chaos would occur in the model due to the time-delay effects and the strong nonlinearity. However, numerical integration of the equations of motion revealed only periodic and quasiperiodic motions, and Moon concluded that a two degree-of-freedom model might be required to observe chaos.

Using perturbation methods and bifurcation theory, Nayfeh et al. (1997) restudied the model built by Hanna and Tobias. Using the method of multiple scales, a normal form of the Hopf bifurcation was obtained by including the effects of the quadratic and cubic nonlinearities. Using a six-term harmonic balance solution, two cyclic-fold bifurcations were found to result in large-amplitude periodic solutions, hysteresis, jumps, and subcritical instability. As the width of cut w increased, the periodic solutions underwent a second Hopf bifurcation, leading to a two-period quasi-periodic motion (a two-torus). The periodic and quasiperiodic solutions were verified using numerical simulation. As w increased further, the torus doubled. Then, the doubled torus broke clown, resulting in a chaotic motion.

However, the effect of the intermittent cut on the nonlinearity of the process has not been adequately treated. In conventional nonlinear models of machining, the cutting is continuous. The dynamics of system can then be described by a nonlinear differential equations with nonlinear delayed terms. The state of the system is continuous as a function of time. But for interrupted machining, the cutting is not continuous, and the state of system is not continuously changing. Instead, the system is described by a two-stage map. In conventional model of continuous cutting, only Hopf bifurcations are

possible. But in interrupted machining, not only Hopf bifurcations, but period-doubling bifurcations are also possible to occur at certain conditions. Actually, with other parameters fixed, the Hopf bifurcations and period-doubling bifurcations occur alternatively with the increase of the spindle speed. In this paper, for the first time, both Hopf and period-doubling bifurcations of interrupted machining are analytically studied.

In Chapter 2, we develop a nonlinear theory for the interrupted machining. Based on the linear theory of Davies et al. (1999a) on interrupted turning and low immersion end-milling, a nonlinear model is built. The system is represented by a single degree-of-freedom system, too, but with a nonlinear delay term. The cutting force is a digressive function of the chip thickness. From this model, the analytic solution of the stability is obtained. Both Hopf and period-doubling bifurcations are found and analyzed. The following section summarized the contributions of this thesis.

Section 1.4: Contributions

- An nonlinear model of interrupted machining is built. The machine tool structure
 is represented by an equivalent single degree of freedom system with the cutting
 forces by a digressive function (α) of chip thickness.
- 2. For highly interrupted machining, the system is simplified as an impact model and an analytic solution is obtained. Besides Hopf bifurcation, Period-doubling bifurcation is also found in interrupted machining. The number of stability lobes is doubled as in the linear results of Davies et al. (1999a).

- 3. The stability chart is analytically estimated using the nonlinear model. In the linear model of Davies et al. (1999a), the feed rate f_0 did not affect the stability of the system, but because of the nonlinearity of the digressive cutting force, f_0 plays a role in determining the stability chart of the nonlinear model. Compared to linear model, the stability lobes of nonlinear model are pulled down. Thus, stability lobes of linear model are misleading, and can lead to false sense of security.
- 4. Both Hopf bifurcation and period-doubling bifurcation are subcritical as $0<\alpha<1$. The effect of the value of α on the bifurcations is analyzed. When $0<\alpha<1$, the bifurcation is subcritical; when $\alpha=1$, the system becomes linear, and the chatter amplitude would be infinite; when $\alpha>1$, the bifurcation is supercritical.
- 5. The additional nonlinearity is introduced by which the vibrating tool leaves the workpiece frequently as the bifurcation occurs. Post-bifurcation orbits are analyzed. Period-two orbits and quasiperiodic orbits are predicted. Possible routes to chaos are discussed.
- 6. Numerical simulations verify the analytic results above. Hysteresis is found for subcritical bifurcations. The stable period-two orbit and quasiperiodic orbit are found and well agree with the analytic solution.

CHAPTER 2

THEORETICAL ANALYSIS

Section 2.1: Modeling of the Interrupt Cutting

2.1.1: Basic Assumptions

To derive the theory for the stability of intermittent machining, two example problems will be considered: turning of a workpiece with a raised area as shown in Figure (2.1); and low-immersion end-milling with an N-fluted end-mill as shown in Figure (2.2). In each case the spindle speed is Ω , measured in revolutions per second (RPM), and the spindle period T is defined to be the inverse of the spindle speed. S is the feed rate in meters per second. For each case, the following assumptions are made.

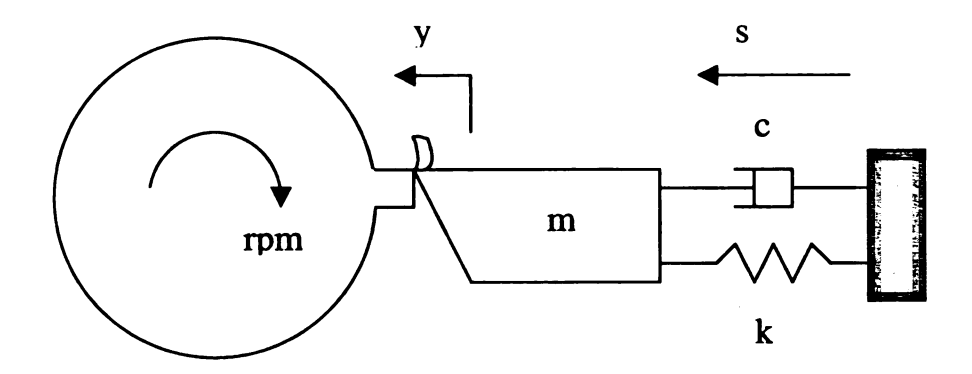


Figure 2.1 Schematic of an interrupted turning operation.

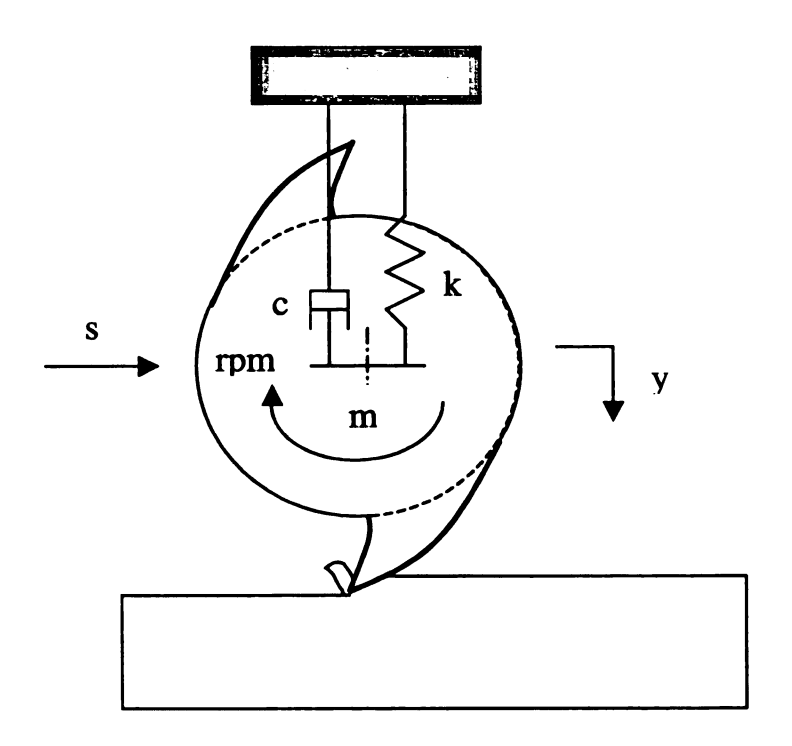


Figure 2.2 Schematic of a low immersion milling operation.

Machine Tool Structure. For the sake of simplicity it will be assumed that
the mode of vibration of the machine tool structure which under certain
conditions may become unstable can adequately be represented by an
equivalent single degree of freedom system, specified by an equivalent mass
m, an equivalent dashpot, and an equivalent spring.

It will further be assumed that the structure can vibrate only in the direction normal to the machined surface and that hence the machine tool system can be represented by models of the type shown in Figure 2.1 for turning and Figure 2.2 for end-milling.

- a. Stiffness. According to Shi and Tobias (1984), there are two sources of nonlinearity. Firstly, by the chatter amplitudes exceeding a certain value, dependent on the mean chip thickness and the vibrating tool leaving the workpiece. Secondly, by a non-linearity of the cutting force characteristics. Machine tool structural nonlinearity has less effect on finite amplitude instability. So here we assume that the stiffness function is linear.
- b. Damping. In high-speed machining, machine tool structural damping is often very small. Usually the damping ratio is a few percent, and frequently less than one percent (Davies (1999)). So here we assume the damping function is also linear and represented by the damping ratio ζ .
- 2. Cutting Force Function. The normal cutting force is assumed to be a digressive function of the chip thickness (Stephan, (1999)), which can be expressed as:

$$F = CK_{,d}^{\alpha} \tag{2.1}$$

Where F is the cutting force, d is the chip thickness, K_t is the generalized thrust cutting force coefficient which is proportional to the width of cut w, and $0<\alpha<1$. C is determined by other cutting conditions. The relation between the cutting force and the chip thickness is shown in Figure 2.3:

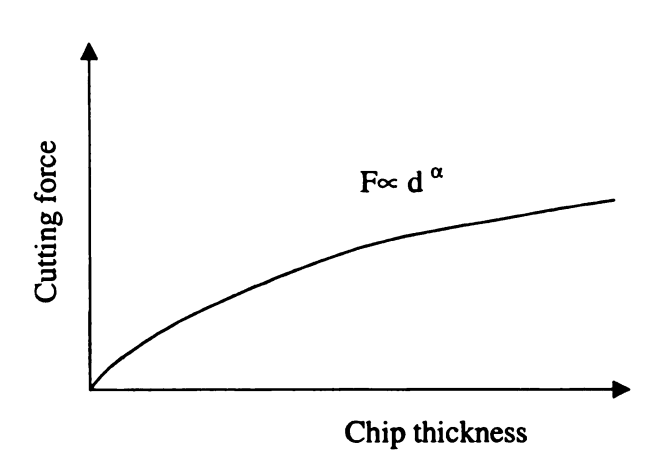


Figure 2.3 The relation between cutting force and chip thickness

3. Very small immersion ratio ρ . The time of contact is a small fraction of the period for one engagement between the workpiece and the tool, and is very small compared to the characteristic response time of the system.

Assumptions 1 and 2 are similar to those models built by previous researchers. Assumption 3 is the key to the approximate analytical solution presented later. Next, we will derive the equation of motions for turning and milling respectively.

2.1.2: Modeling of Interrupted Turning

A simple form of interrupted cutting operation is the turning of a small raised area on a round workpiece as shown in figure 2.1. For simplicity, all flexibility is assumed to be perpendicular to the workpiece surface (y-direction). The *i*th revolution of the workpiece is defined to be begin at time $t_{i-1} = (i-1)T$. During this revolution, cutting begins at time $t_i^- = (i-\rho)T$ and ends at time $t_i^- = iT$. Applying the assumption 1 and 2, the equation of motion is written as:

$$m\ddot{y} + c\dot{y} + ky = -K_{,w}d^{\alpha} \tag{2.2}$$

m— equivalent mass of the system;

c — damping coefficient of equivalent dashpot;

k — stiffness coefficient of equivalent spring;

 K_t — thrust force coefficient, where the negative sign before it is introduced to allow for the opposite directions in which increases of y and d are measured;

w — axial depth of chip or chip width;

d — radial depth of chip or chip thickness, and it is given by the following relations.

$$d = 0, t \in ((i-1)T, i(1-\rho)T) d = f_0 + y(t) - y(t-T), t \in (i(1-\rho)T, iT)$$
 (2.3)

T — tool engagement period, which is the inverse of spindle speed Ω in interrupted turning and $1/N\Omega$ in low immersion milling, where N is the number of flutes on the endmill;

 f_0 — feed per engagement and $f_0 = ST$;

y(t) — current displacement of the tool

y(t-T) — displacement of the tool during the previous engagement.

By using damping ratio ζ and natural frequency of the system ω_n , the equation (2.2) becomes,

$$\ddot{y} + 2\zeta\omega_n\dot{y} + \omega_n y = -\frac{K_i w}{m}d^{\alpha}$$
 (2.4)

where

$$\zeta = \frac{c}{2\sqrt{km}}; \quad \omega_n = \sqrt{\frac{k}{m}}$$
 (2.5)

The component of velocity in the y-direction is defined as,

$$v(t) = \dot{y}(t) \tag{2.6}$$

For the *i*th revolution of the workpiece, the solution of equation (2.4) proceeds as follows. At time t_{i-1} , the position and velocity of the system are denoted (y_{i-1}, v_{i-1}) . This serves as an initial condition for equation (2.4) with the chip thickness d set to zero according to equation (2.3). The system undergoes a simple damped, harmonic oscillation until time t_i^- . At this time, the new position and velocity are denoted (y_i^-, v_i^-) . This serves as the initial condition for equation (2.4) with non-zero chip thickness. The solution then proceeds until time t_i^- resulting in the new position and velocity (y_i, v_i) , which is then used as the initial condition for the next revolution (i+1). The procedure begins with some set of initial conditions at time t_0^- and proceeds ad-infinitum with repetition of the above-mentioned steps. Thus the solution for each revolution defines a two-stage map taking conditions (y_{i-1}, v_{i-1}) to (y_i, v_i) . The first stage of the map has an analytic time-domain solution. In general, the second does not.

2.1.3: Modeling of Low Immersion Milling

For the most simplified case, low immersion endmilling operations produce equations whose stability can be approximately determined by studying equations (2.2) and (2.3). To see this, consider the low immersion endmilling operation shown schematically in Figure 2.2. Making the assumption that the horizontal and vertical (y-direction) motions are not coupled through the machine tool structure (i.e., diagonal mass, damping, and stiffness matrices) and applying assumption 3, the following equations of motion for the cutter are obtained (see Davies et al. [30]):

$$\ddot{y} + 2\zeta \omega_n \dot{y} + \omega_n^2 y = -\frac{K_i w}{m} d^{\alpha}$$
 (2.7)

where

$$d = 0, t \in ((i-1)T, i(1-\rho)T)$$

$$d \approx y(t) - y(t-T), t \in (i(1-\rho)T, iT)$$
(2.8)

Compared to equations (2.3) and (2.4), the only difference here is that equation (2.8) is absent a feed-rate determined driving term that does not directly affect the stability of the system. Thus for very small ρ , the approximate stability behavior of low immersion milling is the same as that for the interrupted turning.

Section 2.2: Approximate Analytic Solution

In this section, we derive an approximate time-domain solution for interrupted cutting operations. The key to the analytic stability calculation is to find an approximate solution for the map describing the evolution of the interrupted cutting. The map must be

developed in two phases: (1) the free vibration phase that maps the state (y_{i-1}, v_{i-1}) to the state (y_i^-, v_i^-) ; and (2) the cutting or delayed forcing phase that maps the state (y_i^-, v_i^-) to the state (y_i^-, v_i^-) . We begin by considering interrupted turning. Low immersion milling can be treated in a similar manner.

For *i*th revolution, the free vibrations evolve according to the state-transition matrix for a damped harmonic oscillator (see Hirsch and Smale (1974)). Given the state at the end of cut number i-1, denoted (y_{i-1}, v_{i-1}) , the state at the beginning of cut number i, denoted (y_i^-, v_i^-) is given by the following expression:

$$\begin{pmatrix} y_i^- \\ v_i^- \end{pmatrix} = A \begin{pmatrix} y_{i-1} \\ v_{i-1} \end{pmatrix} \tag{2.9}$$

where A is the state-transition matrix and can be expressed as follows:

$$A = e^{-\zeta \omega_n \tau} \begin{pmatrix} \frac{\zeta \omega_n}{\omega_d} \sin(\omega_d \tau) + \cos(\omega_d \tau) & \frac{1}{\omega_d} \sin(\omega_d \tau) \\ -\frac{\omega_n^2}{\omega_d} \sin(\omega_d \tau) & \cos(\omega_d \tau) - \frac{\zeta \omega_n}{\omega_d} \sin(\omega_d \tau) \end{pmatrix}$$
(2.10)

where

$$\omega_d = \omega_n \sqrt{1 - \zeta^2} \tag{2.11}$$

which is the damped natural frequency for the free oscillator, and

$$\tau = (1 - \rho)T \tag{2.12}$$

which is the transition time. This fully describes the evolution of the system form the initial state to the state just prior to the engagement with the workpiece.

The derivation of an approximate solution for the second portion of the map taking (y_i^-, v_i^-) to (y_i^-, v_i^-) requires the use of assumption 3. Its validity is supported by a

comparison of the approximate order of magnitude of the system response time at the onset of instability (given by the inverse of the classical chatter frequency) and the order of magnitude of the time of contact as the fractional time-of-contact ρ is decreased.

The response time of the system can be estimated using the expression for the chatter frequency for the case where $\rho = 1$. For $\zeta << 1$, Tobias (1964) shows that this frequency can be approximated by,

$$\omega_{\lim} = \sqrt{2\frac{K_t w_c}{m} + \omega_n^2} \tag{2.14}$$

where $\omega_{\rm lim}$ is the chatter frequency and $\omega_{\rm lim}$ is the critical width-of-cut for instability in the case where $\rho=1$; note that $\omega_{\rm lim}$ is a function of the spindle speed and thus the chatter frequency changes as we sweep along the traditional lobe diagram. Using equation (2.14), the approximate response time of the system, denoted \bar{t} , is given by $\frac{2\pi}{\omega_{\rm lim}}$. Empirically, it has been observed that as the immersion ρ decreases, the critical

width-of-cut scales as $\frac{1}{\rho}$ at all spindle speeds (Davies et al. 1999a). This observation, when combined with equation (2.14) suggests that the characteristic period of the system should scale as $\frac{1}{\sqrt{\rho}}$ for small ρ . However, ρ is a linear function of the time of contact.

Therefore as ρ decreases, the time of contact decreases more rapidly than the characteristic period of the system. This implies that for ρ small enough, the tool can be assumed to remain at a fixed position during each subsequent cut. The surface location resulting from each cut is determined by the position of the tool when the cut is commenced. The velocity of the tool changes in response to the finite impulse it

experiences during the cut. Thus assumption 3 greatly simplifies the dynamics of the tool, and allows an analytic solution to be obtained for the stability of the system.

Assume that the position of the oscillator remains constant during the cutting interaction so that $y_i = y_i^-$ and keep in mind that ρ is very small, the cutting forces are impulses simplified as shown in Figure 2.4. So the approximate velocity of the system after the cut can be found by using the impact model (Davies et al. (1999)),

$$(v_i - v_i^-) = -\frac{K_i \rho w}{m\Omega} (f_0 + y_i^- - y_{i-1})^{\alpha}$$
 (2.16)

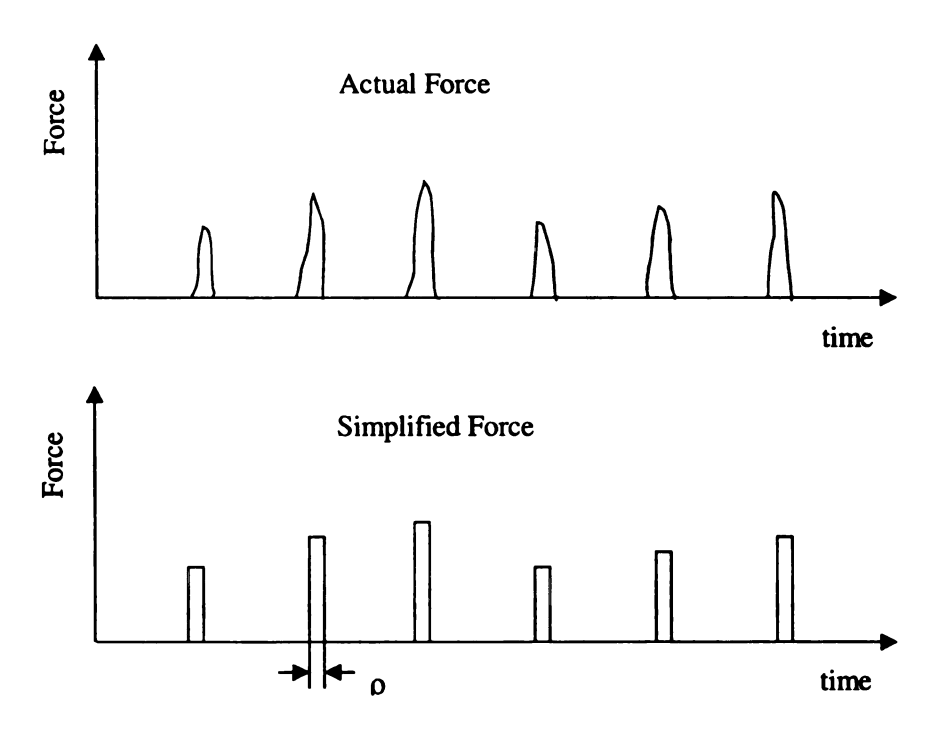


Figure 2.4 Cutting force series in interrupted machining

Applying these assumptions we obtain the following expression for the second portion of the map in matrix form,

$$\begin{pmatrix} y_i \\ v_i \end{pmatrix} = \begin{pmatrix} y_i^- \\ v_i^- \end{pmatrix} + \begin{pmatrix} 0 \\ -\frac{K_i \rho w}{m\Omega} (f_0 + y_i - y_{i-1})^{\alpha} \end{pmatrix}$$
 (2.17)

Combining equations (2.9) and (2.17),

$$\begin{pmatrix} y_i \\ v_i \end{pmatrix} = A \begin{pmatrix} y_{i-1} \\ v_{i-1} \end{pmatrix} + \begin{pmatrix} 0 \\ -\frac{K_i \rho w}{m\Omega} (f_0 + y_i - y_{i-1})^{\alpha} \end{pmatrix}$$
 (2.18)

A similar treatment of low immersion milling produces a map with same stability behavior as equation (2.18) with the relevant engagement period now being $\frac{1}{N\Omega}$ instead of $\frac{1}{\Omega}$ and with f_0 set to zero. The map thus has the form,

$$\begin{pmatrix} y_i \\ v_i \end{pmatrix} = A \begin{pmatrix} y_{i-1} \\ v_{i-1} \end{pmatrix} + \begin{pmatrix} 0 \\ -\frac{K_i \rho w}{m\Omega} (y_i - y_{i-1})^{\alpha} \end{pmatrix}$$
 (2.19)

This form makes physical sense since we expect that for very low immersion milling, the periodic driving term is very small, but displacements in the sensitive direction y still produce substantial changes in the force. Thus, both systems are modeled by a kicked harmonic oscillator with delay. Next we will determine the stability of this model. Since the interrupted turning is a simplified model of low immersion milling and they are qualitatively similar in dynamics, the rest of this work focuses on the analysis of equation (2.18).

Section 2.3: Local Stability

To determine the stability of the equation (2.18), the fixed point of the map is first determined and then the stability of motions about that fixed point are examined. A fixed point (\hat{y}_i, \hat{v}_i) remains unchanged on further iteration of the map. So in equation (2.18), let

$$\begin{pmatrix} y_i \\ v_i \end{pmatrix} = \begin{pmatrix} y_{i-1} \\ v_{i-1} \end{pmatrix} = \begin{pmatrix} \hat{y} \\ \hat{v} \end{pmatrix}$$
 (2.20)

We can get

$$\begin{pmatrix} \hat{y} \\ \hat{v} \end{pmatrix} = (I - A)^{-1} \begin{pmatrix} 0 \\ -\frac{K_t \rho w}{m\Omega} f_0^{\alpha} \end{pmatrix}$$
 (2.21)

where I is the identity matrix. The fixed point represents a forced periodic motion of the tool with period T in turning and $\frac{T}{N}$ in milling. The local stability of this periodic motion is determined by the linearization of the map about the fixed point.

To get the linearization of the map, we Taylor-expand the nonlinear term of equation (2.18), and keep the first four terms to get

$$-\frac{K_i \rho w}{m\Omega} (f_0 + y_i - y_{i-1})^{\alpha} \approx c_0 + c_1 (y_i - y_{i-1}) + c_2 (y_i - y_{i-1})^2 + c_3 (y_i - y_{i-1})^3$$
 (2.22)

where

$$c = -\frac{K_{t}\rho w}{m\Omega};$$

$$c_{0} = cf_{0}^{\alpha};$$

$$c_{1} = c\alpha f_{0}^{\alpha-1};$$

$$c_{2} = c\alpha(\alpha - 1)f_{0}^{\alpha-2};$$

$$c_{3} = c\alpha(\alpha - 1)(\alpha - 2)f_{0}^{\alpha-3}$$

$$(2.23)$$

Substituting equation (2.22) into the equation (2.18), and rearranging it, yields

$$\begin{pmatrix} y_i \\ v_i \end{pmatrix} = B \begin{pmatrix} y_{i-1} \\ v_{i-1} \end{pmatrix} + \begin{pmatrix} 0 \\ c_0 + c_2 (y_i - y_{i-1})^2 + c_3 (y_i - y_{i-1})^3 \end{pmatrix}$$
 (2.24)

where the matrix B is defined as

$$B = \begin{pmatrix} A_{11} & A_{12} \\ A_{21} + c_1(1 - A_{11}) & A_{22} - c_1 A_{12} \end{pmatrix}$$
 (2.25)

where A_{11} , A_{12} , A_{21} , A_{22} are elements of Matrix A.

We make a coordinate transformation to shift the fixed point to the origin:

$$\begin{pmatrix} y_i \\ v_i \end{pmatrix} = \begin{pmatrix} \widetilde{y}_i \\ \widetilde{v}_i \end{pmatrix} + \begin{pmatrix} \widehat{y} \\ \widehat{v} \end{pmatrix}$$
 (2.26)

Substituting into equation (2.24), we get a new equation,

$$\begin{pmatrix} \widetilde{y}_i \\ \widetilde{v}_i \end{pmatrix} = B \begin{pmatrix} \widetilde{y}_{i-1} \\ \widetilde{v}_{i-1} \end{pmatrix} + \begin{pmatrix} 0 \\ c_2(\widetilde{y}_i - \widetilde{y}_{i-1})^2 + c_3(\widetilde{y}_i - \widetilde{y}_{i-1})^3 \end{pmatrix}$$
 (2.27)

whose equilibrium is (0,0). For simplification, we drop the " \sim " in equation (2.27)and write it as,

$$\begin{pmatrix} y_i \\ v_i \end{pmatrix} = B \begin{pmatrix} y_{i-1} \\ v_{i-1} \end{pmatrix} + \begin{pmatrix} 0 \\ c_2(y_i - y_{i-1})^2 + c_3(y_i - y_{i-1})^3 \end{pmatrix}$$
 (2.28)

This is the equation we will deal with in the rest of this work. The stability of the fixed point of equation (2.28) is determined by the eigenvalues of matrix B. Particularly, if either of the eigenvalues of B lies outside of the unit circle in the complex plane (i.e., has magnitude greater than 1), then the magnitude of any perturbation about the fixed points will grow without bound on further iteration of the map; the system is unstable. Conversely, if both eigenvalues lie within the unit circle, all perturbations about the fixed point will decay to zero if given enough iterations; the system is stable (Devaney (1987),

Moon (1992)). When one or both of the eigenvalues of B lies on the unit circle, the stability is borderline, and parameters that cause this to occur lie on the stability boundary for the system.

Note the eigenvalues of matrix B are functions of chip width w. So for a given system, if all the other parameters are fixed, there must be a limit chip width, denoted as w_{\lim} . When $w < w_{\lim}$, the eigenvalues lie in the unit circle and the cutting is stable; when $w > w_{\lim}$, one of the eigenvalues or both eigenvalues lie outside of the unit circle and the cutting becomes unstable.

The linear stability has been analyzed by Davis et al. (1999a), and B adopted through the rest of this section is for the case of digressive cutting forces.

The eigenvalues of B are calculated from the characteristic equation and can be written as:

$$\lambda^2 - Tr(B)\lambda + |B| = 0 \tag{2.29}$$

where λ are the eigenvalues of B, and Tr(B) and |B| are the trace and determinant of B, respectively. It can be shown that Tr(B) and |B| can be expressed relatively simply in terms of the components of the matrix A and the width of cut as follows:

$$Tr(B) = Tr(A) - c_1 A_{12}$$

 $|B| = |A| - c_1 A_{12}$ (2.30)

Without any further analysis, a useful conclusion can be drawn from equation (2.30): for values of the parameters such that $A_{12} = 0$ the characteristic equation for the system reduces to the equation for a damped simple harmonic oscillator, and the system

is stable. Examining equation (2.10), and defining $2\pi f_d = \omega_d$, where f_d is the damped frequency in HZ, and ω_d is the damped frequency in radius per second, we see that $A_{12} = 0$ when the following condition is satisfied:

$$N\Omega = \frac{2f_d(1-\rho)}{n}$$
 $n = 1, 2, 3, \cdots$ (2.31)

Recall that N is the number of flutes for the milling problem and is equal to 1 for interrupted turning. Thus, for an interrupted cutting operation with small ρ the most stable engagement frequencies are approximately $2f_d$, f_d , $\frac{2f_d}{3}$, $\frac{f_d}{2}$... Alternate $(n=2,4,6,\cdots)$ stable speeds f_d , $\frac{f_d}{2}$, $\frac{f_d}{3}$,... are recognized as approximately the same as the optimally stable speeds for a full immersion machining operation. However, the frequencies $2f_d$, $\frac{2f_d}{3}$, $\frac{2f_d}{5}$... $(n=1,3,5,\cdots)$, are new stable speeds not predicted for full immersion cutting. These new stable speeds were tested and experimentally and numerically verified by the theory of partial immersion machining presented in Davies et al. (1999b).

An exact stability criterion can be derived from further analysis of equation (2.29). There are three possible ways for the system to become unstable: (1) a real-valued eigenvalue passes through positive one travelling to the right on the real-axis; (2) a real-valued eigenvalue passes through negative one traveling to the left on the real-axis; and (3) a complex-conjugate eigenvalue pair passes outside the unit circle in the complex plane. Stability criteria can be determined simply by examining the implications of these conditions on equation (2.29). Each case will now be considered separately.

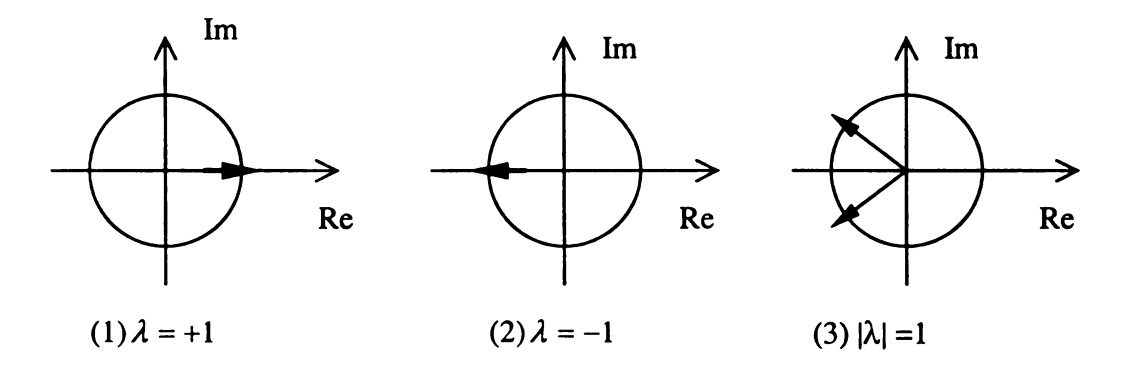


Figure 2.5 The ways the eigenvalues travel through the unit circle

Case 1: $\lambda = +1$

Setting $\lambda = +1$ in equation (2.29) produces the following equation.

$$1 - Tr(A) + |A| = 0 (2.32)$$

This equation is independent of the width-of-cut w, and cannot be satisfied for non-trivial values of the parameters. Thus, $\lambda = +1$ is not a route to instability for this system.

Case 2: $\lambda = -1$

Setting $\lambda = -1$ in equation (2.29) and noting that $|A| = e^{\frac{-2\zeta\omega_n(1-\rho)}{\Omega}}$ and that $Tr(A) = 2e^{\frac{-\zeta\omega_n(1-\rho)}{\Omega}}\cos(\frac{\omega_n(1-\rho)}{\Omega})$, the following expression relating w_{\lim} and Ω can be derived.

$$w_{\text{lim}} = \frac{1}{\alpha f_0^{\alpha - 1}} \cdot \frac{m\Omega \omega_d}{\rho K_t} \cdot \frac{\cosh(\zeta \omega_n \frac{1 - \rho}{\Omega}) + \cos(\omega_d \frac{1 - \rho}{\Omega})}{\sin(\omega_d \frac{1 - \rho}{\Omega})}$$
(2.33)

The numerator of equation (2.33) is always positive. Thus, requiring w_{lim} to be positive, implies that the sin term in the denominator must be positive. This occurs for values of Ω in intervals defined as follows:

$$\frac{\omega_d(1-\rho)}{(2k+1)\pi} < \Omega < \frac{\omega_d(1-\rho)}{2k\pi} \qquad k = 1, 2, 3, \dots$$
 (2.34)

For all other values of Ω , w_{lim} is infinite or negative; these cases are non-physical and are disregarded.

Case 3: $\lambda \overline{\lambda} = 1$

This case can be related as $\lambda \overline{\lambda} = 1$, where $\overline{\lambda}$ is the complex conjugate of λ . This condition implies that |B| = 1. Applying this condition, another expression relating w_{\lim} to Ω can be derived:

$$w_{\text{lim}} = \frac{1}{\alpha f_0^{\alpha - 1}} \cdot \frac{-2m\Omega\omega_d}{\rho K_t} \cdot \frac{\sinh(\zeta\omega_n \frac{1 - \rho}{\Omega})}{\sin(\omega_d \frac{1 - \rho}{\Omega})}$$
(2.35)

The numerator of equation of (2.35) is always negative implying that, to obtain positive values of w_{lim} , the values of Ω must be in the following intervals:

$$\frac{\omega_d(1-\rho)}{2k\pi} < \Omega < \frac{\omega_d(1-\rho)}{(2k-1)\pi} \qquad k = 1,2,3,\cdots$$
 (2.36)

At speeds where $\sin\left(\frac{w_d(1-\rho)}{\Omega}\right) = 0$, equations (2.33) and (2.35) imply infinite

stability. This is consistent with the observation made above that the characteristic equation reduces to that of the damped simple harmonic oscillator at these speeds.

Taken together equation (2.33) and (2.35) provide expressions for those combinations of w and Ω that produce borderline stability in the system. Plots of these parameter values as demonstrated in Figure 2.6 are analogous to the stability lobe diagrams for uninterrupted machining.

For example, consider the interrupted turning of an aluminum workpiece as shown in Figure 2.1. For the purpose of illustration, let us assume the following reasonable parameter values for the modal stiffness, mass and damping of the cutting tool: k=1 MN/m, m=0.05 kg, c=8.9 N-s/m, $f_0=0.1$ mm/revolution. This gives a damped natural frequency of 711 Hz and a damping ratio 2%. In addition, assuming a reasonable value for K_t of 500 N/mm², $\alpha=0.41$ and $\rho=2\%$, the stability lobe diagram can be calculated from equations (2.33) and (2.35).

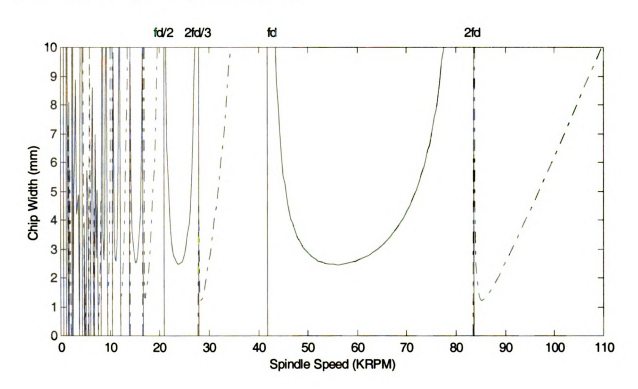


Figure 2.6 Stability lobes diagram of interrupted turning

Figure 2.6 shows the stability lobes of the interrupted cutting system over a wide range of spindle speeds (some obviously not attainable). The lobes determined by equation (2.33) are represented with dotted line and the lobes determined by equation (2.35) are represented with a solid line. The asymptotes at $\frac{2f_d}{n}$ are clearly visible as large narrow regions of stability. Note that in contrast to traditional regenerative chatter stability where the highest speed stable region is at a spindle speed equal to dominant frequency of the system, the last optimally stable region for interrupted machining is at twice that frequency.

Traditional regenerative chatter theory predicts that for a single degree of freedom system the most stable speeds are at integer fractions of the natural frequency of the system (i.e. $\frac{f_n}{k}$, $k=1,2,3,\cdots$). The new theory predicts a set of stable speeds based on fractions of the damped natural frequency defined by $\frac{2f_d(1-\rho)}{k}$, $k=1,2,3,\cdots$. For small damping and small ρ , a subset of these stable speeds are approximately the same as those predicted by the traditional theory. The others are not. A plausible physical explanation of these new speeds is as follows. In partial immersion machining, the location of the surface is determined by the location of the tool when it makes the cut. Stable machining is most likely to occur when the tool returns to the same location at the beginning of each cut. This can occur in two ways: (1) the period of the spindle is an integer multiple of the period of the tool $\frac{1}{f_d}$ indicating stable spindle speeds of

 $\frac{f_d}{k}$, $k=1,2,3,\cdots$; or (2) the period of the spindle is an odd integer multiple of one half of the period of the tool $\frac{1}{2f_d}$ indicating stable speeds of $\frac{2f_d}{k}$, $k=1,3,5,\cdots$. Taken together these stable speeds are approximately those given by equation (2.33) and (2.35). This is an appealing and easily remembered "rule of thumb".

The type of instability, or more formally the form of the bifurcation that leads to instability is different for the two types of lobes. On the lobes shown by the solid lines, the instability results forma pair of complex eigenvalues passing through the unit circle in the complex plane. In the dynamics literature, this is known as Hopf bifurcation. This is same type of bifurcation that occurs in traditional regenerative chatter theory. On the lobes shown by the dotted lines, the bifurcation occurs as a real eigenvalue passes through minus one. This type of bifurcation known as a period-doubling bifurcation has not been previously been observed in machining. This implies that the post chatter behavior will be different depending on the spindle speed. Experimentally it was observed as a difference in the sound of the chatter by Davies et al. (1999b).

While this type of interrupted turning operation is relatively rare, interrupted milling operations are common. Davies et al. (1999b) demonstrated in a simple experiment that the theory presented applies to practical milling operations as well.

Section 2.4: Local Bifurcations

To study the bifurcation of the map with one parameter changing, we assume that all parameters, except the chip width, w, are fixed. We consider the period-doubling bifurcation and Hopf bifurcation respectively.

Case 1: Period-doubling bifurcation

From Figure 2.6, we can see, those stability lobes act as the critical limits for both the chip width and spindle speed. It is also called the parameter space in dynamics. If we fix the spindle speed Ω at a certain value, the dynamics change with the chip width w, which causes bifurcation. To make the problem simple, we choose the spindle speed Ω to lie approximately at the middle of each lobe. As such gives the lowest limit chip width w_{lim} at each lobe for Hopf bifurcation (Tlusty (1986)).

$$\Omega_k = \frac{\omega_d (1 - \rho)}{(2k + \frac{1}{2})\pi} \qquad (k = 0, 1, 2, \dots)$$
 (2.37)

When k=0, $\Omega_0 = \frac{2\omega_d(1-\rho)}{\pi}$, corresponding to the last lobe, and the biggest lobe for the period-doubling bifurcation at the right hand side of stability diagram. The parameter traces are shown in Fiugre 2.7.

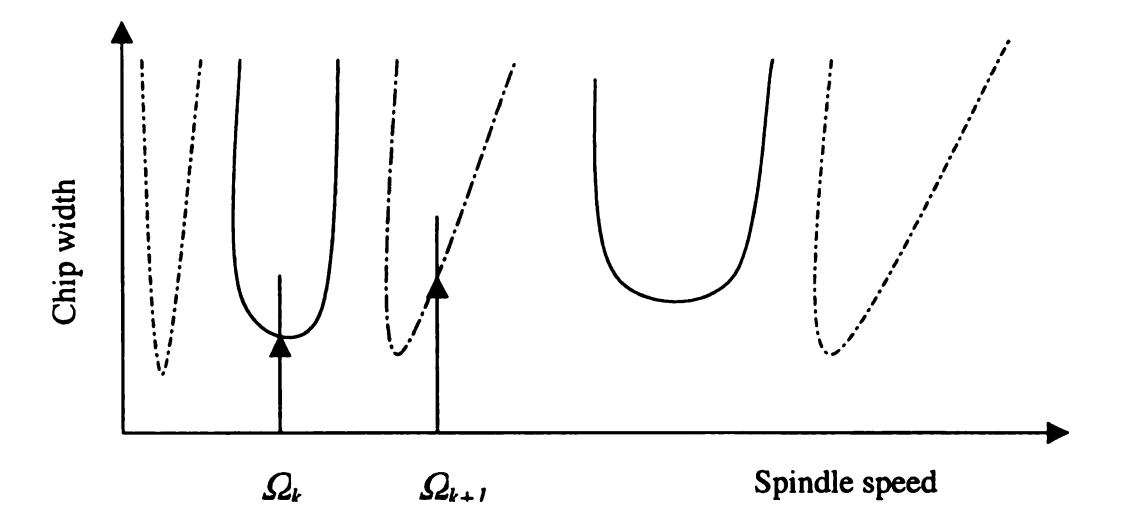


Figure 2.7 Parameter traces for bifurcations

With the spindle speed Ω fixed at Ω_k , matrix A becomes:

$$A_{k} = e^{\frac{\zeta}{\sqrt{1-\zeta^{2}}}(2k+\frac{1}{2})\pi} \begin{pmatrix} \frac{\zeta\omega_{n}}{\omega_{d}} & \frac{1}{\omega_{d}} \\ -\frac{\omega_{n}^{2}}{\omega_{d}} & -\frac{\zeta\omega_{n}}{\omega_{d}} \end{pmatrix}$$
(2.38)

The limit chip width where the bifurcation occurs becomes w_k , where

$$w_{k} = \frac{m}{\rho K_{t}} \cdot \frac{1 - \rho}{(2k + \frac{1}{2})\pi} \cdot \frac{\omega_{d}^{2}}{\alpha f_{0}^{\alpha - 1}} \cdot \cosh(\frac{\zeta}{\sqrt{1 - \zeta^{2}}} (2k + \frac{1}{2})\pi)$$
(2.39)

and consequently, the coefficient c_1 becomes

$$c_{1,k} = \omega_d \cdot \cosh(\frac{\zeta}{\sqrt{1-\zeta^2}} (2k + \frac{1}{2})\pi)$$
 (2.40)

To use the suspension trick of center-manifold theory, we split c_I in two parts as

$$c_1 = c_{1,k} + \mu \tag{2.41}$$

Considering $\mu(y_i - y_{i-1})$ as a nonlinear term, then equation (2.28) become:

where

$$B_{k} = \begin{pmatrix} A_{11} & A_{12} \\ A_{21} + c_{1,k} (1 - A_{11}) & A_{22} - c_{1,k} A_{12} \end{pmatrix}$$
 (2.43)

Notice that the eigenvalues of B_k are -1 and λ_2 , ($|\lambda_2| < 1$), and c_2 , c_3 are linear functions of μ .

To simplify equation (2.42), we use the transformation

$$\begin{pmatrix} y \\ v \end{pmatrix} = T \cdot \begin{pmatrix} x \\ u \end{pmatrix} \tag{2.44}$$

where T is composed of the eigenvectors of B_k . The equation (2.42) becomes

$$\begin{pmatrix} x_i \\ u_i \end{pmatrix} = J \cdot \begin{pmatrix} x_{i-1} \\ u_{i-1} \end{pmatrix} + \begin{pmatrix} f(x_{i-1}, u_{i-1}, \mu) \\ g(x_{i-1}, u_{i-1}, \mu) \end{pmatrix}$$
 (2.45)

where J is the Jordan form of the matrix B_k :

$$J = \begin{pmatrix} -1 & 0 \\ 0 & \lambda_2 \end{pmatrix} \tag{2.46}$$

Writing the center-manifold in the form

$$u = h(x, \mu) = a_1 x^2 + a_2 x \mu + a_3 \mu^2$$
 (2.47)

then the dynamics on the center-manifold are

$$x_{i} = -x_{i-1} + f(x_{i-1}, h(x_{i-1}, \mu), \mu)$$
 (2.48)

Substitute equation (2.47) and (2.48) into (2.45), solve for a_1 , a_2 , a_3 , we can obtain the map on the center-manifold:

$$x \mapsto -x + b_1 \mu x + b_2 x^2 + b_3 \mu x^2 + b_4 \mu^2 x + b_5 x^3 + O(4)$$
 (2.49)

where b_1 , b_2 , b_3 , b_4 , and b_5 are constants. O(4) means the fourth order or higher in variables x and μ , which are infinitesimal around the origin.

The normal form of this map is:

$$x \mapsto -x + b_1 \mu x + b_2 x^3 + O(4)$$
 (2.50)

The sign of $\frac{b_r}{b_1}$ determines the types of the bifurcation and the stability of the period-two

orbit. When $\frac{b_r}{b_1} > 0$, the bifurcation is subcritical, and the period-two orbit is unstable.

When $\frac{b_r}{b_1} < 0$, the bifurcation is supercritical, and the period-two orbit is stable (Wiggins, (1990)).

The dominant form of the relation between b_1 , b_r and the parameters like ζ , ω_d , α can not be obtained, we turn to use some examples to show the bifurcation.

We use the same example as in Figure 2.6, the interrupted turning operation with the parameters m=0.05kg, k=1MN/m, c=8.9N-s/m, $f_0=0.1mm/revolution$, and $\zeta=2\%$, $f_n=711Hz$, $\rho=2\%$, $\alpha=0.41$, $K_l=500N/mm^2$. Fixing the cutting speed at 33.5 krpm, we can get the normal form of the map:

$$x \mapsto -x - 0.000337215 \mu x - 8.79211 \times 10^{-6} x^3 + O(4)$$

So the period-doubling bifurcation here is subcritical, and the period-two orbit is unstable. The bifurcation diagram is shown in Figure 2.8.

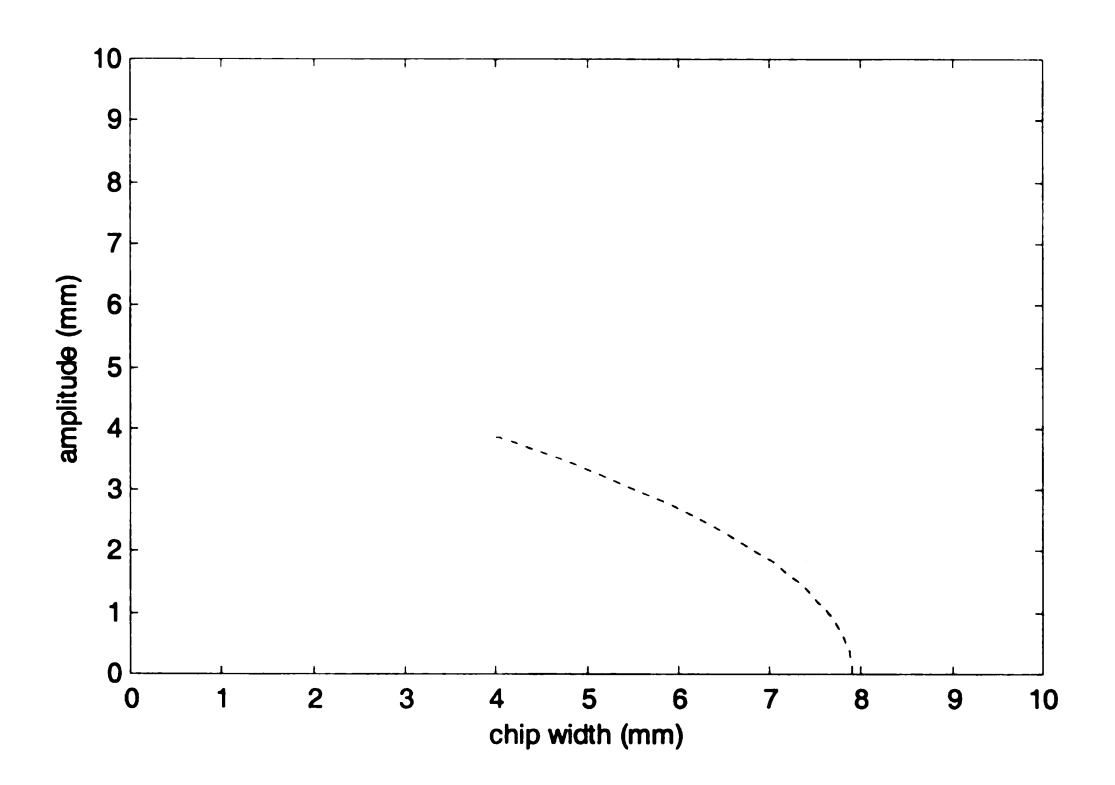


Figure 2.8 Subcritical period-doubling bifurcation diagram.

Case 2: Hopf bifurcation

For the same reason as in the period-doubling bifurcation, we fix Ω at the following values for each of the lobes (as mentioned above, they are corresponding to the lowest chip width, (Tlusty, 1986):

$$\Omega_k = \frac{\omega_d (1 - \rho)}{(2k - \frac{1}{2})\pi} \qquad k = 1, 2, 3, \dots$$
(2.51)

When k=1, $\Omega_1 = \frac{2\omega_d (1-\rho)}{3\pi}$, which is the second to the last lobe, the biggest lobe for the

Hopf bifurcation at the right hand side of stability diagram.

Correspondingly, we get other parameters as A_k , w_k , $c_{1,k}$, B_k , \cdots and similarly,

$$A_{k} = e^{-\frac{\zeta}{\sqrt{1-\zeta^{2}}}(2k-\frac{1}{2})\pi} \begin{pmatrix} -\frac{\zeta\omega_{n}}{\omega_{d}} & -\frac{1}{\omega_{d}} \\ \frac{\omega_{n}^{2}}{\omega_{d}} & \frac{\zeta\omega_{n}}{\omega_{d}} \end{pmatrix}$$
(2.52)

$$w_{k} = \frac{m}{\rho K_{t}} \cdot \frac{1 - \rho}{(2k - \frac{1}{2})\pi} \cdot \frac{2\omega_{d}^{2}}{\alpha f_{0}^{\alpha - 1}} \cdot \sinh(\frac{\zeta}{\sqrt{1 - \zeta^{2}}} (2k - \frac{1}{2})\pi)$$
 (2.53)

$$c_{1,k} = 2\omega_d \cdot \sinh(\frac{\zeta}{\sqrt{1-\zeta^2}}(2k-\frac{1}{2})\pi)$$
 (2.54)

$$B_{k} = \begin{pmatrix} A_{11} & A_{12} \\ A_{21} + c_{1,k} (1 - A_{11}) & A_{22} - c_{1,k} A_{12} \end{pmatrix}$$
 (2.55)

The eigenvalues of B_k take the form

$$\lambda_{1,2} = \cos \beta \pm i \sin \beta \tag{2.57}$$

Transforming the coordinates system as

$$\begin{pmatrix} y \\ v \end{pmatrix} = T \cdot \begin{pmatrix} x \\ u \end{pmatrix} \tag{2.58}$$

where

$$T = \left(e_1, e_2 \begin{pmatrix} 1 & i \\ 1 & -i \end{pmatrix}\right) \tag{2.59}$$

and e_1 , e_2 are eigenvectors of B_k , the equation (2.56) becomes

$$\begin{pmatrix} x_i \\ u_i \end{pmatrix} = \begin{pmatrix} \cos \beta & -\sin \beta \\ \sin \beta & \cos \beta \end{pmatrix} \cdot \begin{pmatrix} x_{i-1} \\ u_{i-1} \end{pmatrix} + \begin{pmatrix} f(x_{i-1}, u_{i-1}, \mu) \\ g(x_{i-1}, u_{i-1}, \mu) \end{pmatrix}$$
 (2.60)

where μ is defined as in case 1.We can transform the above equation into polar coordinates and get the normal form (Guckenheimer and Holmes, (1983)).

$$r \mapsto r + d\mu r + ar^3 + O(4)$$

$$\theta \mapsto \theta + c + br^2 + O(3)$$
(2.61)

The signs of the coefficients a and d determine the direction and stability of the bifurcation periodic orbits; c and b give asymptotic information on rotation numbers.

The invariant circle is expressed as:

$$\left\{ (r,\theta) \in R^+ \times S^1 \middle| r = \sqrt{\frac{-\mu d}{a}} \right\} \tag{2.62}$$

It is asymptotically stable for a < 0 and unstable for a > 0 (Wiggins, (1990)).

Since a and d are the most important for determining the local bifurcation and the periodic orbits, using some shortcuts to compute the a and d directly will let us know the characteristics of the bifurcation immediately. From the process of normalization, we know,

$$d = \frac{d}{d\mu} |\lambda(\mu)|_{\mu=0}$$
 (2.63)

where $\lambda(\mu)$ is the eigenvalue of matrix B.

Rewriting the equation (2.60) as

$$\begin{pmatrix} x \\ y \end{pmatrix} \mapsto \begin{pmatrix} \cos \beta & -\sin \beta \\ \sin \beta & \cos \beta \end{pmatrix} \cdot \begin{pmatrix} x \\ y \end{pmatrix} + \begin{pmatrix} f(x, y, \mu) \\ g(x, y, \mu) \end{pmatrix}$$
 (2.64)

with the eigenvalues $\lambda, \overline{\lambda} = \cos(\beta) \pm \sin(\beta)$. The value of a can be obtained by (Guckenheimer and Holmes, (1983)),

$$a = -\text{Re}\left[\frac{(1-2\lambda)\overline{\lambda}^2}{1-\lambda}\xi_{11}\xi_{20}\right] - \frac{1}{2}|\xi_{11}|^2 - |\xi_{02}|^2 + \text{Re}(\overline{\lambda}\xi_{21})$$
 (2.65)

where

$$\xi_{20} = \frac{1}{8} [(f_{xx} - f_{yy} + 2g_{xy}) + i(g_{xx} - g_{yy} - 2f_{xy})]$$

$$\xi_{11} = \frac{1}{4} [(f_{xx} + f_{yy}) + i(g_{xx} + g_{yy})]$$

$$\xi_{02} = \frac{1}{8} [(f_{xx} - f_{yy} - 2g_{xy}) + i(g_{xx} - g_{yy} + 2f_{xy})]$$

$$\xi_{21} = \frac{1}{16} [(f_{xxx} + f_{xyy} + g_{xxy} + g_{yyy}) + i(g_{xxx} + g_{xyy} - f_{xxy} - f_{yyy})]$$
(2.66)

All the variables above are evaluated at $(x, y, \mu) = (0,0,0)$.

Similarly, the dominant form of the relation between d, a and the parameters like ζ , ω_d , α can not be obtained, we turn to use some examples to show the bifurcation.

We use the same example as in Figure 2.6, the interrupted turning operation with the parameters: m=0.05kg, k=1MN/m, c=8.9N-s/m, $f_0=0.1mm/revolution$, and so $\zeta=2\%$, $f_n=711Hz$, $\rho=2\%$, $\alpha=0.41$, $K=500N/mm^2$. Fix the cutting speed at 55.8krpm, we can get the normal form of the map:

$$r \mapsto r + 34.9892 \mu r + 1.61396 \times 10^{-6} r^3$$

So the Hopf bifurcation here is subcritical, and the period orbit is unstable. The bifurcation diagram is shown in Figure 2.9.

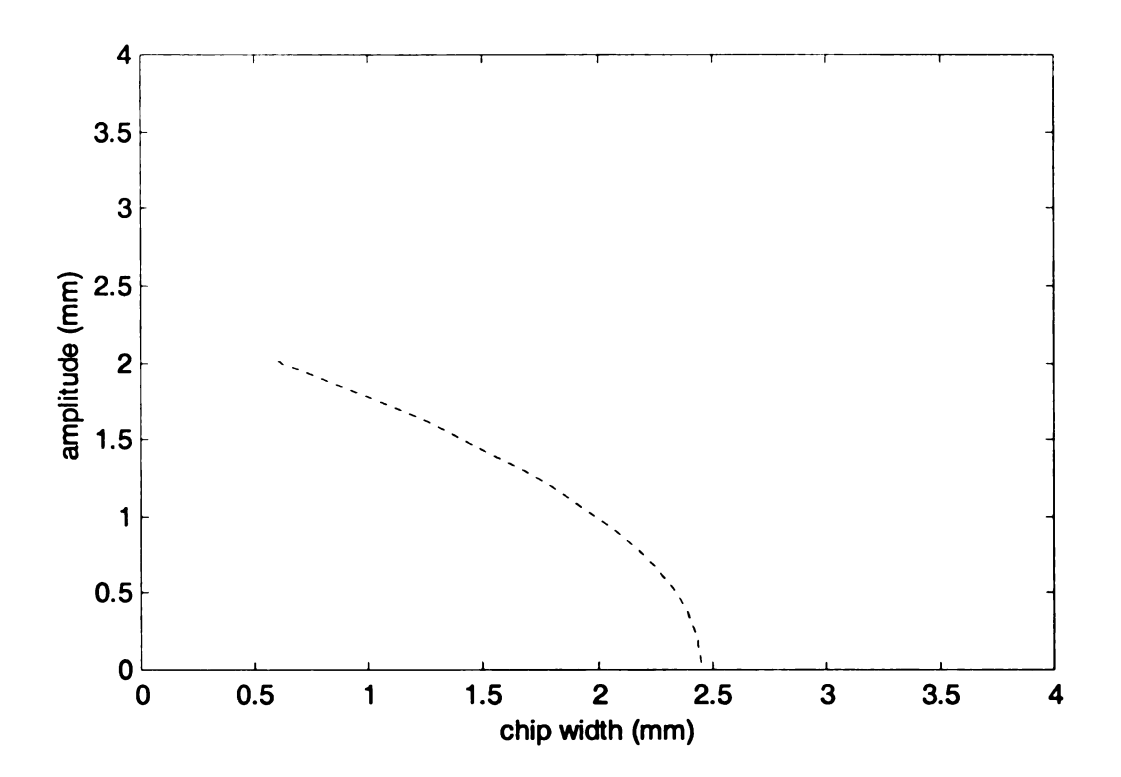


Figure 2.9 Subcritical Hopf bifurcation diagram

Section 2.5: The Role of α

In this thesis, we assume the cutting force is a digressive function of chip thickness, i.e.

$$F = Cd^{\alpha} \tag{2.67}$$

where F is the force, d is the chip thickness, and C is a constant determined by cutting conditions.

This is an empirical relation between cutting forces and chip thickness. Pratt (1999) showed that $\alpha = 0.41$ in continuous cutting by the experiments. This makes sense since when chip thickness d is very small, cutting force F increases quickly with the

increase of d; but when d becomes bigger, F increases more and more slowly with the increase of d. This is a material property. The relation between F and d can not be linear in real cutting. Actually the value of α has important role on stability and it determines the subcritical/supercritical bifurcation.

We rewrite the equation (2.28) as

$$\begin{pmatrix} y_i \\ v_i \end{pmatrix} = A \begin{pmatrix} y_{i-1} \\ v_{i-1} \end{pmatrix} + \begin{pmatrix} 0 \\ c_1(y_i - y_{i-1}) + c_2(y_i - y_{i-1})^2 + c_3(y_i - y_{i-1})^3 \end{pmatrix}$$
 (2.68)

where c_1 , c_2 , c_3 are functions of α

To investigate the role of α on the bifurcations, fixed all parameter values, so that A, c are constants, (Note, c<0), and c_1 , c_2 and c_3 are only functions of α . From equation (2.68), we can see that c_1 determines the linear part of the map, so it determines the critical bifurcation point. In the stability chart, for a given spindle speed, c_1 determines the limit chip width, w_{lim} .

Reviewing the equation (2.33) and (2.35), with all parameter values fixed, the value of w_{lim} is only function of α . When $\alpha = 1$,

$$w_{\text{lim}} = \frac{m\Omega\omega_d}{\rho K_l} \cdot \frac{\cosh(-\zeta\omega_n \frac{1-\rho}{\Omega}) + \cos(\omega_d \frac{1-\rho}{\Omega})}{\sin(\omega_d \frac{1-\rho}{\Omega})}$$

$$\frac{\omega_d (1-\rho)}{(2k+1)\pi} < \Omega < \frac{\omega_d (1-\rho)}{2k\pi} \qquad k = 1,2,3,\dots$$
(2.69)

$$w_{\lim} = \frac{-2m\Omega\omega_d}{\rho K_t} \cdot \frac{\sinh(\zeta\omega_n \frac{1-\rho}{\Omega})}{\sin(\omega_d \frac{1-\rho}{\Omega})}$$
(2.70)

$$\frac{\omega_d(1-\rho)}{2k\pi} < \Omega < \frac{\omega_d(1-\rho)}{(2k-1)\pi} \qquad k = 1,2,3,\cdots$$

which are exactly the results of the linear model investigated by Davis (1999a). For $0 < \alpha < 1$, the term $\frac{1}{\alpha f_0^{\alpha-1}}$ is always smaller than 1, so w_{lim} from the nonlinear model is always smaller than the corresponding one from the linear model. In figure 2.10, the stability charts of two cases: $\alpha = 0.41$ and $\alpha = 1$, are compared. It can be seen that the stability charts from the nonlinear model are lower than those from linear model. This partly explains why the threshhold of stability predicted by a linear model can not be set up in actual experiments. The stability charts predicted by a nonlinear model is closer to experimentally determined stability charts than the ones predicted by a linear model.

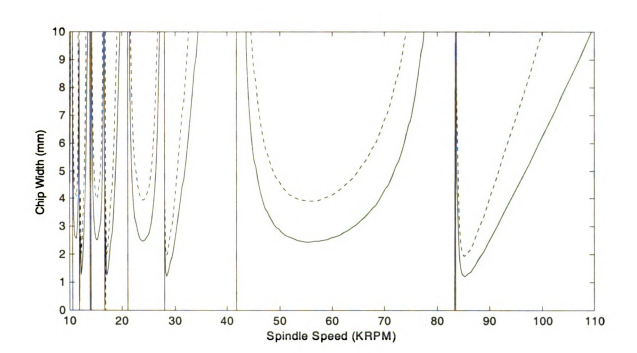


Figure 2.10 The comparison of stability charts from the nonlinear model and the linear model. (---- linear model, — nonlinear model)

To see the role of α on subcritical/supercritical bifurcations, let us review the process of simplification and normalization of the map (2.28).

For period-doubling bifurcation, the normal form is:

$$x \mapsto -x + b_1 \mu x + b_r x^3 + O(4)$$

Comparing it with equation (2.68), and reviewing the process in Section 2.4, we can imply that b_1 is totally determined by c_1 , i.e.

$$b_1 = f(c_1) (2.71)$$

Actually, with all parameter values fixed,

$$b_1 = f(\alpha f_0^{\alpha - 1}) \tag{2.72}$$

 b_r is determined by c_2 and c_3 , i.e.

$$b_r = f(c_2, c_3) (2.73)$$

Note, $\alpha f_0^{\alpha-1} > 0$ for all $\alpha > 0$, so b_1 may not change the sign when α goes from [0,1] to $[1,\infty]$. But c_2 and c_3 may change their signs and therefore b_r may change its sign, so the bifurcation may change from subcritical to supercritical when α goes from [0,1] to $[1,\infty]$. Because the dominant form of the relation between b_r and α can not be obtained, we demonstrate several cases of the value of α .

For example, the interrupted turning operation with the parameters, m=0.05kg, k=1MN/m, c=8.9N-s/m, f_0 =0.1mm/revolution, and therefore ζ =2%, ω_n =711Hz, ρ =2%, K=500N/mm². Fix cutting speed at 33.5krpm, try the following values of α , we get the corresponding normal forms.

 $\alpha = 0.11, \qquad -x - 0.000337215 ux - 0.0000102382 x^3$ $\alpha = 0.41, \qquad -x - 0.000337215 ux - 8.79211 \times 10^{-6} x^3$ $\alpha = 0.90, \qquad -x - 0.000337215 ux - 2.04524 \times 10^{-6} x^3$ $\alpha = 1.00, \qquad -x - 0.000337215 ux$ $\alpha = 1.10, \qquad -x - 0.000337215 ux + 2.27179 \times 10^{-6} x^3$ $\alpha = 1.20, \qquad -x - 0.000337215 ux + 4.77012 \times 10^{-6} x^3$ $\alpha = 2.00, \qquad -x - 0.000337215 ux + 0.0000329126 x^3$

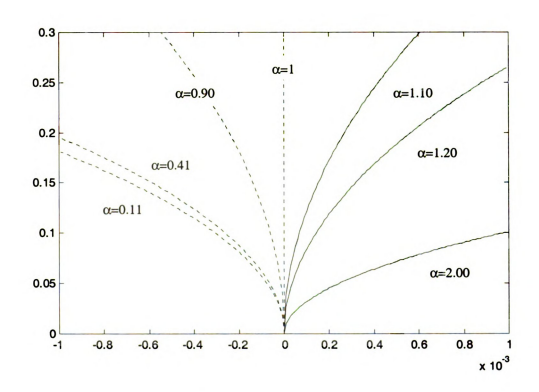


Figure 2.11 Period-doubling bifurcation diagrams at different values of α

Figure 2.11 showes the bifurcation diagrams at different values of α , From the diagrams, we can see that, when $0 < \alpha < 1$, the period-doubling bifurcation is subcritical, and the period-two orbits are unstable, so the hysteresis will happen; when $\alpha > 1$, which is not physically possible, the period-doubling bifurcation would be supercritical, and the period-two orbits would be stable, and there would be no hysteresis. When $\alpha = 1$, the system degrades to a linear model. The chatter amplitude tends to go to infinity, in contradiction to "the finite amplitude instability" theory. This is why a linear model is not sufficient to describe the system when bifurcations occur.

For Hopf bifurcations, the role of α is similar. The normal form is

$$r \mapsto r + d\mu r + ar^3 + O(4)$$

where d is totally determined by c_1 , i.e.

$$d = f(c_1) \tag{2.74}$$

Actually, with all parameter values fixed,

$$d = f(\alpha f_0^{\alpha - 1}) \tag{2.75}$$

a is determined by c_2 and c_3 , i.e.

$$a = f(c_2, c_3) (2.76)$$

Similarly, d may not change the sign when α goes from [0,1] to $[1,\infty]$, but a may change its sign, so the bifurcation may change from subcritical to supercritical. Because the dominant form of the relation between a and α can not obtained, we try several cases of the value of α . We use same example of the interrupted turning operation. Fixing the cutting speed at 55.8krpm, applying the following values of α , we get the corresponding normal forms.

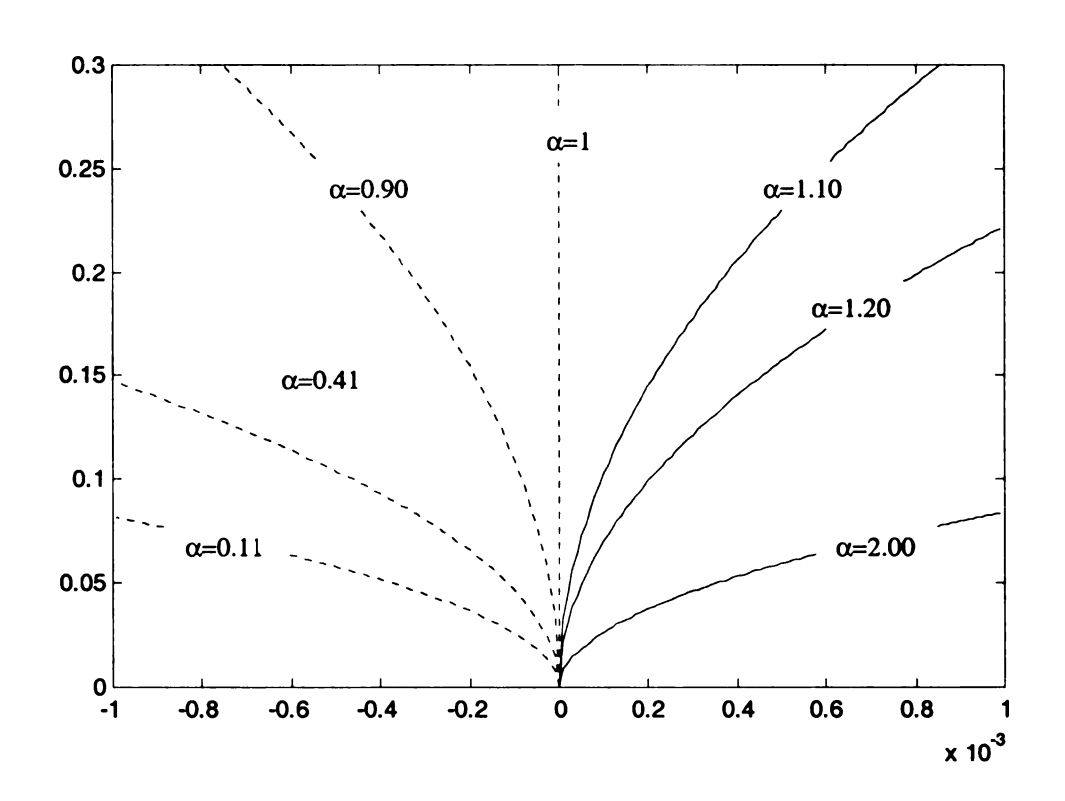


Figure 2.12 Hopf bifurcation diagrams at different values of $\boldsymbol{\alpha}$

Figure 2.12 showes the Hopf bifurcation diagrams at different values of α . We can see that, when $0 < \alpha < 1$, the Hopf bifurcation is subcritical, and the tori are unstable, so hysteresis will happen; when $\alpha > 1$, which is not physically possible, the Hopf bifurcation would be supercritical, and the tori would be stable, and there would be no hysteresis. When $\alpha = 1$, the system degrades to a linear model. The chatter amplitude tends to go to infinite, in contradiction to "the finite amplitude instability" theory. Again the linear model is not sufficient to describe the system when bifurcations occur.

Section 2.6: Post-Bifurcation Orbits

2.6.1 Global Considerations

Local considerations are sufficient for understanding the consequences of a supercritical bifurcation, which is a continuous bifurcation, while global considerations are necessary to understand the consequences of a subcritical bifurcation, which is a catastrophic bifurcation.

When a subcritical period-doubling bifurcation takes place, the branch of stable periodic solutions that exists before the bifurcation (say $w < w_{lim}$) continues as an unstable branch of periodic solutions after the bifurcation (at $w = w_{lim}$). An unstable limit cycle (period-two orbit) collides with the stable limit cycle (period-one orbit), and the two are replaced with an unstable limit cycle of the lower period. The local state of the dynamical system will be an attracting limit cycle for $w < w_{lim}$. However, for $w > w_{lim}$, the post-bifurcation state of the system cannot be determined by local considerations alone; global

considerations are necessary. There are two possibilities. First, the system evolution may be attracted to a remote solution, which is either bounded (fixed point, periodic solution, quasiperiodic solution, chaos) or unbounded. Such a bifurcation is dangerous and is typically accompanied by hysteresis. Second, the system response may explode into a new attractor (possibly chaos) when w is slowly varied past w_{lim} , with the old attractor being a proper subset of the new attractor. The transition from a periodic state to a chaotic state following a subcritical period-doubling bifurcation has been termed intermittent transition of type III to chaos by Pomeau and Manneville (1980).

When a Hopf bifurcation takes places, the branch of stable periodic solutions that exists prior to the Hopf bifurcation continues as a branch of unstable periodic solutions after the bifurcation. A quasiperiodic orbit collides with the period-one orbit, and the two are replaced with an unstable limit cycle of the period-one. The local state of the dynamical system will be an attracting limit cycle for $w < w_{lim}$. However, for $w > w_{lim}$, the post-bifurcation state of the system cannot be determined by local considerations alone; global considerations are necessary. Similarly, there are two possibilities. First, the system evolution may be attracted to a distant solution, which is either bounded (point, periodic, quasiperiodic, or chaotic attractor) or unbounded. Second, the state of the system may explode into a larger attractor, with the old attractor being a proper subset of the new attractor. The transition from a periodic state to a chaotic state following a subcritical Hopf bifurcation has been termed **intermittent transition of type II to chaos** by Pomeau and Manneville (1980).

2.6.2 Case 1. Period-doubling Bifurcation

As explained in section 2.6.1, when the system undergoes the subcritical period-doubling bifurcation as the chip width exceeds the threshold value w_{lim} , the post-bifurcation state of the system cannot be determined by local considerations alone. Global considerations are necessary. What are the global considerations here specifically in low immersion milling?

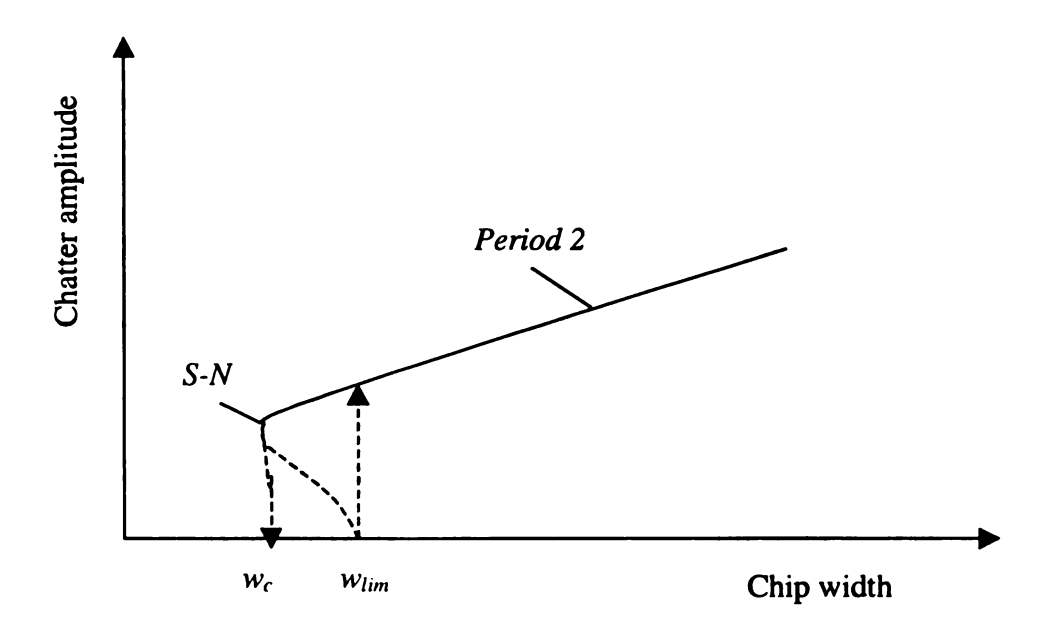


Figure 2.13 Bifurcation diagram for Hopf bifurcation in continuous cutting (S-N: Saddle-Node bifurcation)

According to "finite amplitude instability" theory, the model of continuous machining is based on the assumption that the tool will not leave the cut. The Hopf bifurcation occurs after the chip width w becomes bigger than the threshold value $w_{\rm lim}$, and the "jump phenomenon" occurs. The amplitude of oscillation increases suddenly and because of the nonlinearity of system, it will stabilize at a period-two orbit if the chip thickness is big enough. This is shown in Figure 2.13 which is a Hopf bifurcation diagram for continuous machining.

In low immersion milling, the amplitude "jump" in the subcritical period-doubling bifurcation would cause the tool leaves the cut (run-out) immediately! This makes sense because the immersion ratio is so small that the chip thickness is very small, even a small increase in oscillation amplitude would cause the tool run-out.

What does it mean when the tool leaves cut? It means the tool does not engage in cut during the subsequent revolution for interrupted turning, and the mill does not engage in cut for the subsequent tooth for low immersion milling. What should be cut off by this tooth will be left there and be cut off by the following tooth. Since the machine keeps feeding in, the following tooth will cut off more than what it would otherwise cut. This causes a bigger cutting force and results possibly in intensified oscillations. At the same time, since the every other tooth does not engage in cut, the tool has more time to dampen the oscillation, actually approximately twice the time as usual. It means the transition time for the free vibration doubled. So there is a trend that the oscillation will be damped more. There is a trade-off between these two effects—for example, the stable period-two orbit may be created! This period-two orbit is characterized by "cut, no cut, cut, no cut....." for every other tooth in low immersion milling and every other revolution in interrupted turning.

The simulations for period-two orbits in Chapter 3 will show this scenario. To prove it theoretically, first we assume this period-two orbit exist, then we prove that it is stable.

Basically this period-two orbit is the same as to the period-one orbit except that the transition time (for free vibration) doubled.

We can write the similar map as:

$$\begin{pmatrix} y_{i+1} \\ v_{i+1} \end{pmatrix} = A^{(2)} \begin{pmatrix} y_{i-1} \\ v_{i-1} \end{pmatrix} + \begin{pmatrix} 0 \\ -\frac{K_t \rho w}{m\Omega} (2f_0 + y_{i+1} - y_{i-1})^{\alpha} \end{pmatrix}$$
 (2.67)

$$A^{(2)} = e^{-\zeta \omega_n \tau} \begin{pmatrix} \frac{\zeta \omega_n}{\omega_d} \sin(\omega_d \tau) + \cos(\omega_d \tau) & \frac{1}{\omega_d} \sin(\omega_d \tau) \\ -\frac{\omega_n^2}{\omega_d} \sin(\omega_d \tau) & \cos(\omega_d \tau) - \frac{\zeta \omega_n}{\omega_d} \sin(\omega_d \tau) \end{pmatrix}$$
(2.68)

where

$$\tau = (2 - \rho)T = \frac{2 - \rho}{\Omega}$$
 (2.69)

The fixed point of map (2.67) corresponds to a period-two orbit on the Poincare section.

$$\begin{pmatrix} y_{i+1} \\ v_{i+1} \end{pmatrix} = \begin{pmatrix} y_{i-1} \\ v_{i-1} \end{pmatrix} = \begin{pmatrix} \hat{y} \\ \hat{v} \end{pmatrix}$$
 (2.70)

Substituting (2.70) into equation (2.67), we get the fixed point for the period-two orbits:

$$\begin{pmatrix} \hat{y} \\ \hat{v} \end{pmatrix} = (I - A^{(2)})^{-1} \begin{pmatrix} 0 \\ -\frac{K_t \rho w}{m\Omega} (2f_0)^{\alpha} \end{pmatrix}$$
 (2.71)

Expanding the nonlinear term in Map (2.67) into a Taylor series leads to

$$-\frac{K_i \rho w}{m\Omega} (2f_0 + y_i - y_{i-1})^{\alpha} \approx c_0 + c_1 (y_i - y_{i-1}) + c_2 (y_i - y_{i-1})^2 + c_3 (y_i - y_{i-1})^3 \quad (2.72)$$

where c_0 , c_1 , c_2 , c_3 are similar to those in the period-one map.

Combining the linear term $c_1(y_i - y_{i-1})$ with matrix $A^{(2)}$ in equation (2.67), and transforming coordinates so that the fixed point of period-two orbit is relocated at origin, we get the following map which is similar to the map for period-one orbit:

$$\begin{pmatrix} y_{i+1} \\ v_{i+1} \end{pmatrix} = B^{(2)} \begin{pmatrix} y_{i-1} \\ v_{i-1} \end{pmatrix} + \begin{pmatrix} 0 \\ c_2 (y_{i+1} - y_{i-1})^2 + c_3 (y_{i+1} - y_{i-1})^3 \end{pmatrix}$$
 (2.73)

where

$$B^{(2)} = \begin{pmatrix} A^{(2)}_{11} & A^{(2)}_{12} \\ A^{(2)}_{21} + c_1 (1 - A^{(2)}_{11}) & A^{(2)}_{22} - c_1 A^{(2)}_{12} \end{pmatrix}$$
(2.74)

Whether the period-two orbit is stable or not is determined by the eigenvalues of matrix $B^{(2)}$. If the absolute value of the eigenvalues of the matrix $B^{(2)}$ are in the unit circle, the period-two orbit is stable; if not, it is unstable.

The eigenvalues of matrix $B^{(2)}$ are functions of chip width w, so the stability of the period-two orbit is determined by the chip width. There is a range of chip widths (w_{\lim}, w_{\lim}) in which the period-two orbit is stable. When $w < w_{\lim}$, the period-two orbit disappears, leaving the period-one orbit, i.e. the fixed point of the original map, as the stable solution. When $w > w_{\lim}$, another bifurcation occurs, and the way the eigenvalues pass through the unit circle determines whether it is a period-doubling bifurcation or Hopf bifurcation.

Furthermore, since the bifurcations from stable cutting are subcritical, the lower limit of chip width for period-two orbit, $w_{\rm lim1}$, must be smaller than the limit chip width for the period-one orbit, $w_{\rm lim}$, which is defined in Section 2.3. i.e.,

$$w_{\rm lim1} < w_{\rm lim}$$

This is the reason why hysteresis happens, this is why we call it catastrophe, and this explains the "jump phenomenon". The figure 2.14 shows the bifurcation diagrams of this case. For the possible chaos, the chatter amplitude can reach any value in the shaded region.

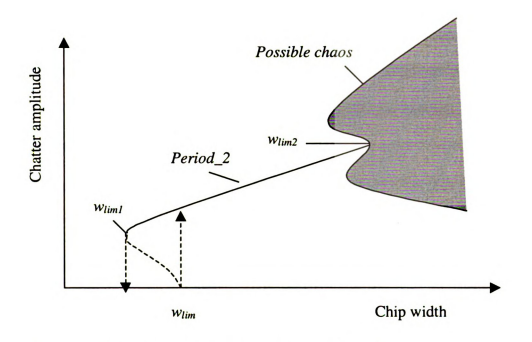


Figure 2.14 Bifurcation diagram for period-doubling bifurcation case

The value of w_{lim2} can be determined by the eigenvalues of matrix $B^{(2)}$ by using the similar method in Section 2.3.

The determination of the value of w_{lim1} needs further global considerations. First, let us assume that the chip thickness (depending on feed rate) is big enough that the tool would never run out of cut during each engagement, even after the period-doubling bifurcation, i.e., the cutting sequence is "cut, cut, cut, cut," for the assumed period-two orbit. The bifurcation diagram of this case is similar to the one in Figure 2.13. Notice that, when $w < w_{lim1}$, the period-one orbit is always stable, and there is a cut during every pass (revolution), and no jump happens. Only after $w > w_{lim1}$, it is possible for the amplitude to jump, depending on the disturbance. After the jump, the chatter amplitude

will be stabilized at the real period-two orbit, which is a sequence of "cut, no cut, cut, no cut.....", before it reaches the assumed period-two orbit. Because the cut-no-cut sequence has more damping time but less impulse than the cut-cut sequence, the amplitude of cut-no-cut sequence must be smaller than the amplitude of cut-cut sequence. There are several possible ways for the chatter amplitude to bifurcate to the real period-two orbit as shown in Figure 2.15.

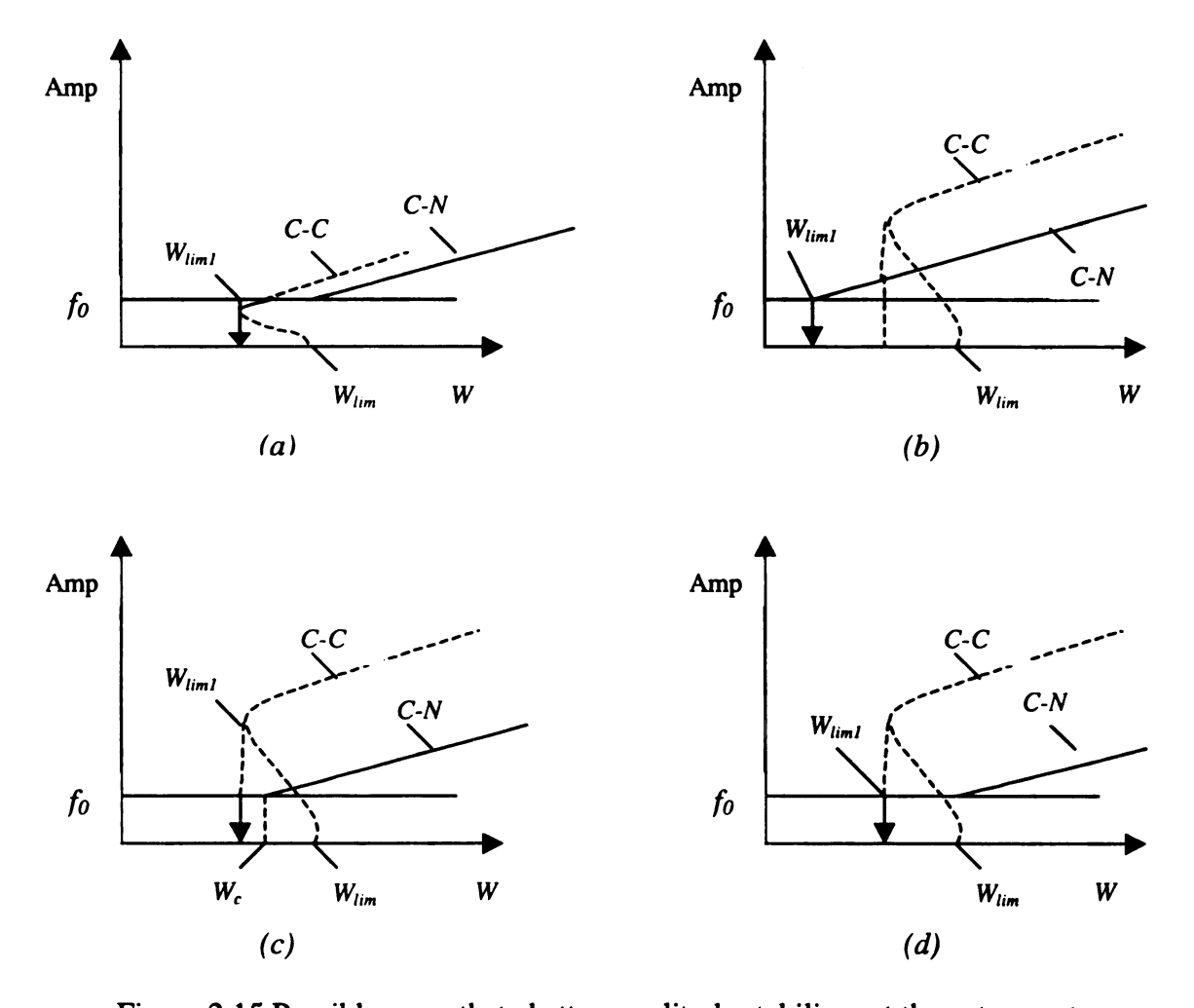


Figure 2.15 Possible ways that chatter amplitude stabilizes at the cut-no-cut period-two orbit. (C-C: Cut-Cut period-two orbit; C-N: Cut-No-cut period-two orbit.)

In Figure 2.15, case (a) is not feasible for low immersion machining because the chip thickness is so small that any jump of the amplitude would cause the tool leave the cut. It is almost impossible to get any stable cut-cut period-two orbit. Case (d) is also not very possible because it assume that the cut-no-cut period-two orbit only exists after $w > w_{lim}$, which is not a physically real case. Case (b) and case (c) are physically possible. In case (c), when $w_{lim1} < w < w_c$, there should be some kind of periodic orbits which are not cut-no-cut period-two orbits. For example, it is possible to be a period-three orbit, like "cut, cut, no cut, cut, cut, no cut......". But we will see in the simulations, that these assumed periodic orbits do not exist for some typical low immersion machining cases. In contrast, the cut-no-cut period-two orbits always exist whenever the "jump" happens. So case (b) is the most physically possible case. In case (b), the w_{lim1} can be determined by the following equation:

$$\hat{y}_2 - \hat{y}_1 = f_0 \tag{2.75}$$

where \hat{y}_2 is the fixed point of the period-two orbit, and \hat{y}_1 is the fixed point of the period-one orbit. This can be explained as following, "as the chip width sweeps backward, the cut-no-cut period-two orbit remains stable. But the amplitude will be smaller and smaller until it reaches the surface of workpiece. After that, the period-two orbit is not of C-N form, and vanishes, leaving the period-one orbit". Substituting equation (2.21) and (2.71) into equation (2.75), we can get,

$$(I - A^{(2)})^{-1} \left(-\frac{K_{\iota} \rho w}{m \Omega} (2f_0)^{\alpha} \right) - (I - A)^{-1} \left(-\frac{K_{\iota} \rho w}{m \Omega} (f_0)^{\alpha} \right) = \begin{pmatrix} f_0 \\ v \end{pmatrix}$$
 (2.76)

where v is an uncertain velocity value.

From equation (2.76), we can get the analytic solution of w_{lim1} as the function of spindle speed Ω , given other parameter values.

For example, we return to the interrupted turning operation with the parameters m=0.05kg, k=1MN/m, c=8.9N-s/m, $f_0=0.1mm/revolution$, and $\zeta=2\%$, $\omega_n=711Hz$, $\rho=2\%$, $\alpha=0.41$ and $K_t=500N/mm^2$. If we fix cutting speed at 33.5krpm, which is the case for period doubling bifurcation in Section 2.4. we can also get the limit chip width for period-one orbit,

$$w_{\lim} = 13.4 \, (mm)$$

The lower limit chip width for the cut-no-cut period-two orbit is:

$$w_{\rm lim1} = 9.9 \, (mm)$$

The upper limit chip width for the cut-no-cut period-two orbit is:

$$w_{\lim 2} = 80.7 (mm)$$

When $w = w_{\lim 2} = 80.7(mm)$, the eigenvalues are:

$$\lambda = -0.4837 + 0.8752i$$
, $\overline{\lambda} = -0.4837 - 0.8752i$

$$|\lambda| = |\overline{\lambda}| = 1$$

So the next bifurcation for the period-two orbit is a Hopf bifurcation. And this Hopf bifurcation is similar to the Hopf bifurcation for the period-one orbit. After this Hopf bifurcation occurs, the system dynamics becomes complicated, perhaps going to chaos as shown in Figure 2.14.

2.6.3 Case 2. Hopf Bifurcation

Now let us consider the post bifurcation state of the system after the Hopf bifurcation occurs for the period-one orbit.

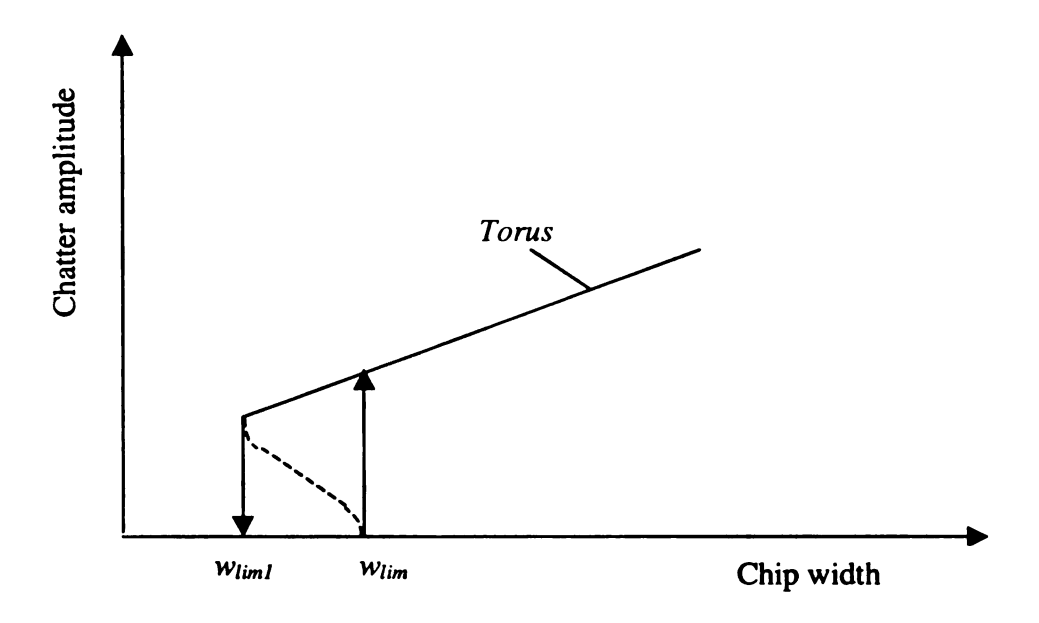


Figure 2.16 Bifurcation diagram for Hopf bifurcation case

Similarly, when the Hopf bifurcation occurs, the cutting will leave the cut, but not so regularly any more. The tool will engage in the cut for several passes, then leave the cut for a couple of passes. The number of passes in cut against the number of passes out of the cut is usually not determined. It depends on the certain value of the chip width and the spindle speed. The state of system can not be represent by an analytic solution as equations (2.67), (2.68) and (2.69), and there are no longer fixed points for period-two orbits. Instead, there is a two-period quasiperiodic orbit (torus) because the newly introduced frequency and the frequency of the periodic orbit that exists prior to the bifurcation are **incommensurate** (two frequencies ω_1 and ω_2 are said to be incommensurate if $\frac{\omega_1}{\omega_2}$ is an irrational number). This quasiperiodic orbit can not be represented by an analytic solution, but can show up in the Poincare section of the period-

two orbits, which should be a closed circle. This will be discussed later in Chapter 3. The bifurcation diagram can be shown in figure 2.16.

Again, because of the hysteresis, for backward sweep, there must be a limit chip width, w_{lim1} that, when $w < w_{lim1}$, the quasiperiodic orbit jumps to the period-one orbit. To find this w_{lim1} , again, we assume the cut-cut period-two orbit exists if the chip thickness is big enough. This is similar to the case of the continuous cutting shown in Figure 2.13. For the cut-cut period-two orbit, at a critical chip width, w_c , a saddle-node bifurcation occurs, and the lower branch of the cut-cut period-two orbit is unstable. But in real machining, before the chatter amplitude stabilizes at the assumed cut-cut period-two orbit, it jumps out of the cut, and the orbit becomes quasiperiodic for the Hopf bifurcation case. The maximum amplitude of the quasiperiodic orbit must be smaller than the cut-cut

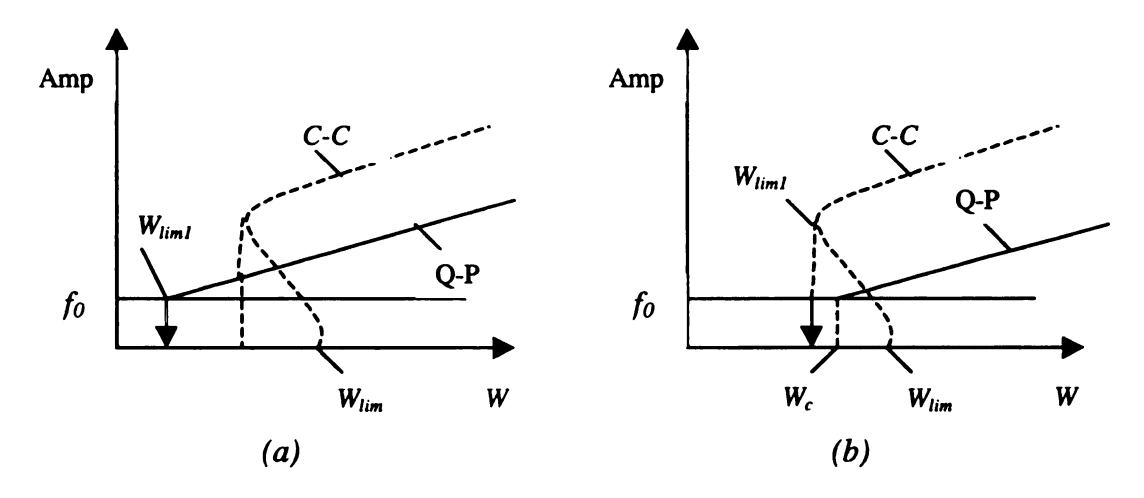


Figure 2.17 Possible ways that chatter amplitude becomes quasiperiodic. (C-C: Cut-Cut period-two orbit; Q-P: Quasi-Periodic orbit.)

period-two orbit. Similar to the period-doubling bifurcation case, there are two physically possible ways for the system becomes quasiperiodic as shown in Figure 2.17. Case (a) is more possible than case (b) as the implications of period-doubling bifurcation. But

because there are no period-two orbits after the Hopf bifurcations. We can not get the analytic solution of $w_{\rm lim1}$. We have to turn to simulations.

Because the range of limit chip width for the stable period-two orbit after the period-doubling bifurcation and the range of limit chip width for the quasiperiodic orbit after Hopf bifurcation are very big compared to the limit chip width for the period-one orbit, and because the immersion ratio is so small in low immersion milling that it can be assumed to be an impulse model, so further studies for bigger chip width are meaningless for the analytic solutions of low immersion milling because the basic assumptions for the impulse model no longer hold. Further studies can be carried out by simulations with the method discussed in Chapter 3.

CHAPTER 3

SIMULATIONS AND EXPERIMENTS

Section 3.1 Simulations

The theoretical aspects of chatter can be well illustrated and understood by using time domain simulation. The time domain simulation of machining operations is to be done for a large number of revolutions at given speed, feed, chip width and other cutting parameters. This approach not only permits a good insight into the behavior of the vibrating system, but also makes it possible to correctly take into account the basic nonlinearity of the process and the effect of perturbations.

The nonlinearity of machining chatter is not only due to the fact that the cutting force is nonlinear function of chip thickness and chip width, but also due to the fact that when vibration grows larger, the tool jumps out of the cut for a part of vibrational period and the cutting force disappears for this time instant.

Specifically, for interrupted turning and low immersion machining, time domain simulation can accurately determine when the tool is in the cut, and when it is out of the cut. That is, it can take into account the global considerations in determining the post-

bifurcation state of the system. So the simulation is a good tool to verify the analytic solutions though it has the drawback that it is specific to a set of parameter values and lacks the versatility and generality of the analytic solution.

3.1.1 Algorithm

Time domain simulation is often time-consuming. Here, to make the algorithm simpler, to well coincide with the analytic model, keeping in mind the assumption that the immersion ratio is so small that the machining operation can always be simplified into an impact model, a simple algorithm can be implemented as following. An initial condition, (y_0, v_0) , evolves through the time $(1-\rho)T$ by using the equation (2.9), and the state becomes (y_i^-, v_i^-) . If the tool is going to engage in cut, the state (y_i, v_i) results from the impact model (equation (2.17)); if not, the state evolves through the time T by free vibration. The simulation process is summarized as below:

(1) Initial conditions (y_0, v_0) ;

(2)
$$\begin{pmatrix} y_i^- \\ v_i^- \end{pmatrix} = A \begin{pmatrix} y_{i-1} \\ v_{i-1} \end{pmatrix}$$
, transition time τ ;

(3) If
$$y_i^- < y_{i-1} + f_0$$
, then $\begin{pmatrix} y_i \\ v_i \end{pmatrix} = \begin{pmatrix} y_i^- \\ v_i^- \end{pmatrix}$, set $\tau = T$; goto (2);

else
$$\begin{pmatrix} y_i \\ v_i \end{pmatrix} = \begin{pmatrix} y_i^- \\ v_i^- \end{pmatrix} + \begin{pmatrix} 0 \\ -\frac{K_i \rho w}{m} (f_0 + y_i - y_{i-1})^{\alpha} \end{pmatrix}$$
, set $\tau = (1 - \rho)T$; goto (2);

3.1.2 Simulations of Stability Lobes

To obtain the stability chart by using time domain simulations is time consuming. Analytical methods are preferred to time domain simulations if the analytical methods are available. Usually, by using time domain simulations, only a certain number of isolated points on the plane of stability chart can be obtained, each of which represents a pair of spindle speed and chip width with other cutting parameters fixed. The stability of these points can be determined by looking at the amplitude of disturbed vibrations. If the amplitude is damping away and finally becomes zero, the point is stable, otherwise it is unstable.

Setting a certain number of pairs of spindle speed and chip width with other parameters fixed, and implementing the simulations using the algorithm above, we can get a set of the unstable points on the plane of the stability chart. The comparison of the analytic solution and the results of time domain simulations are shown in Figure 3.1. From the figure, we can see that the results of the time domain simulations are coincide well with the analytical solutions. The stability lobes of the Hopf bifurcation and the period-doubling bifurcation are verified. Notice that, there are some regions where the stability is conditionally held. It means, they are stable if the disturbance is small, but unstable if the disturbance is big. This will be explained later.

3.1.3 Post Bifurcation Orbits

In chapter 2, we have discussed global bifurcations. After the subcritical period-doubling bifurcation occurs, the tool leaves the cut and a stable period-two orbit is created. The tool will engage in cut with every other tooth (low immersion milling) or every other revolution (interrupted turning). We also find analytical representation for the period-two orbit. After the subcritical Hopf bifurcation occurs, the tool also leaves the cut but not in a periodic way. Instead, a quasiperiodic orbit is created. This quasiperiodic orbit does not have an analytical solution.

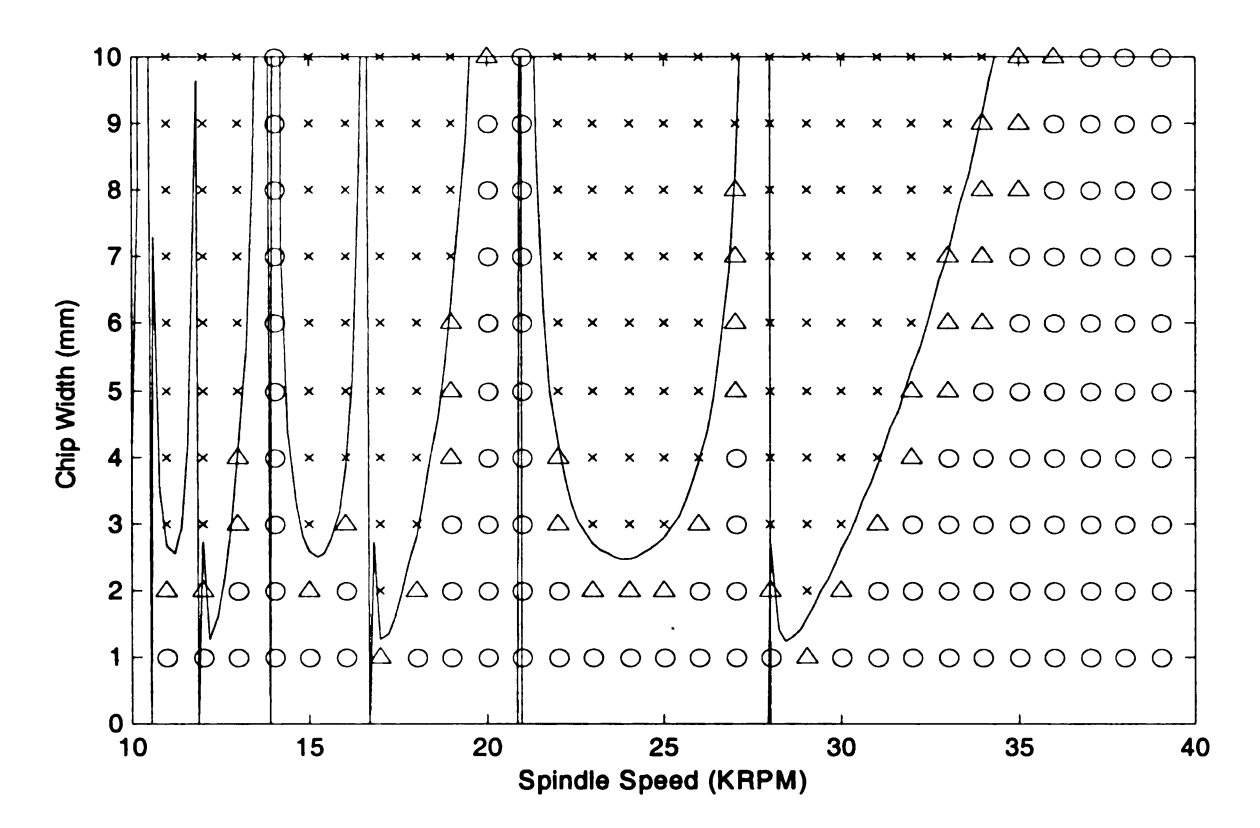


Figure 3.1 Comparison of stability lobes obtained from analytic solutions and from simulations ('x'—unstable points, 'Δ'—conditionally stable points, 'o'—stable points.)

We can use simulations to verify these post-bifurcation orbits.

Because our concern here is only the state of system when the tool engages in the cut during a revolution or a pass, while the system is otherwise just in free vibration, we only record the state at the engagement time for every revolution or pass. We call these records **time series** if they are plotted versus time. With the time series and their **Poincare sections**, we can see the stable period-two orbit and the quasiperiodic orbit.

We return to the same example in chapter 2, the interrupted turning operation with the parameters: m=0.05kg, f₀=0.1mm/revolution, ζ =2%, ω _n=711Hz, ρ =2%, α = 0.41, and K=500N/mm².

Figure 3.2 shows case 1: the stable periodic orbit after the period-doubling bifurcation, where $\Omega = 33.5 krpm$, w = 0.0174m, $(w_{lim} = 0.0134m)$.

Figure 3.3 shows case 2: the quasiperiodic orbit after the Hopf bifurcaiton, where $\Omega = 55.8 krpm$, w = 0.0046m, $(w_{lim} = 0.0042m)$.

In Figure 3.2(a), the peak values of the oscillations represent those passes within the cut; the minimum values represent the passes without a cut. These time series correctly describe the characteristics of post bifurcation state of the system:

cut, not cut, cut, no cut.....

We use the Poincare section to show the characteristics of the orbits. That is, we record the state of the system every revolution or pass at the engaging time. Figure 3.2(b) and Figure 3.3(b) are the Poincare sections corresponding to each case respectively. In figure 3.2(b), only two points can be obtained. One of them is the fixed point for the stable period-two orbit which can also be calculated by using analytic method. Substituting the parameter values used in the simulation into equation (2.70), we get

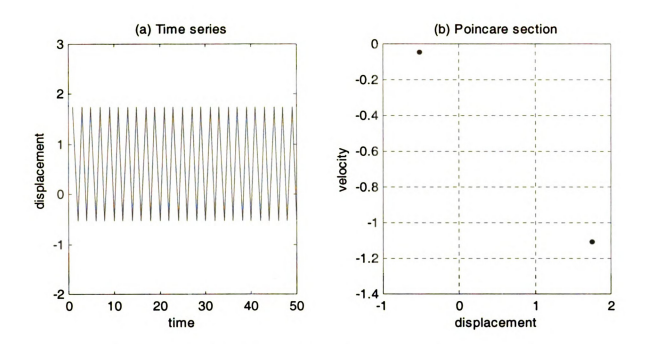


Figure 3.2 Stable period-two orbit after the subcitical period-doubling bifurcation

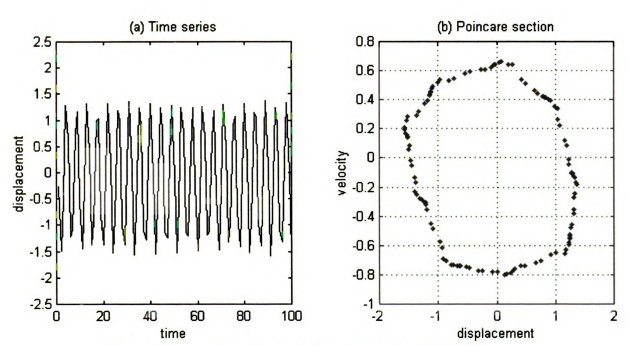


Figure 3.3 Quasiperiodic orbit after the subcitical Hopf bifurcation

$$\begin{pmatrix} \hat{y} \\ \hat{v} \end{pmatrix} = \begin{pmatrix} 1.7524 \\ -1.1048 \end{pmatrix}$$

which is exactly the lower point in figure 3.2(b).

In figure 3.3(a), the time series of the quasiperiodic orbit is shown, which can be depicted in the Poincare section of Figure 3.3(b), in which a closed circle is obtained. To show which passes engage in cut and which passes do not, the tool displacement is plotted versus time along with the instantaneous workpiece surface as in Figure 3.4. the displacements which coincide with the surface represent a cut, and those below the surface are out of the cut.

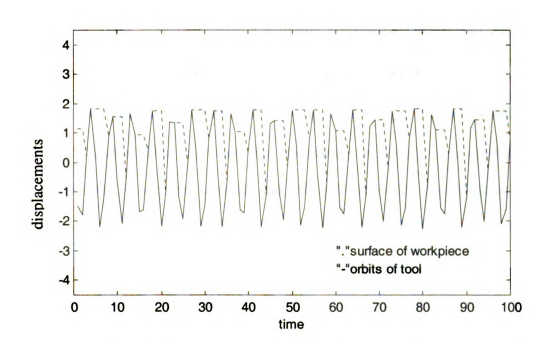


Figure 3.4 Comparison of in-cut passes and out-of-cut passes for quasiperiodic orbits.

3.1.4 Bifurcation Diagram

Using time domain simulations, it is possible to obtain the whole bifurcation diagram from a stable fixed point to periodic orbits, or quasiperiodic orbits, and even to chaos if the algorithm is accurate and simulation time is sufficient. But since here we are concerned the cases around the limit chip width where the local bifurcations occur, we just simulate a certain number of cases near the bifurcation points.

To simulate the bifurcation diagram, we fix the spindle speed at a certain speed, change the chip width little by little, and record the amplitudes of each case. The bifurcation diagrams of simulations are shown in Figure 3.4 and Figure 3.5

From Figure 3.4, we can see that when $w < w_{\text{lim}}$, the period-one orbit is stable. When $w > w_{\text{lim}}$, the subcritical period-doubling bifurcation occurs, and the amplitude jumps from zero to a finite value. There is a range of chip width $(w_{\text{lim1}}, w_{\text{lim2}})$ for which the period-two orbits are stable. When $w_{\text{lim1}} < w < w_{\text{lim}}$, the period-one orbit is conditionally stable. That is, when the disturbance is small, it is stable; when the disturbance is big, it becomes unstable and will stabilize on the period-two orbit. This is called "finite amplitude instability". In experiments, this will be shown as the forward chip width and backward chip width have different jump points.

Figure 3.5 can explained similarly as Figure 3.4. The difference is that after the subcritical Hopf bifurcation occurs, there is no stable period-two orbit. Instead, a two-period quasiperiodic orbit is obtained. Notice that there are some "windows" for chip width in which some periodic orbits might exist.

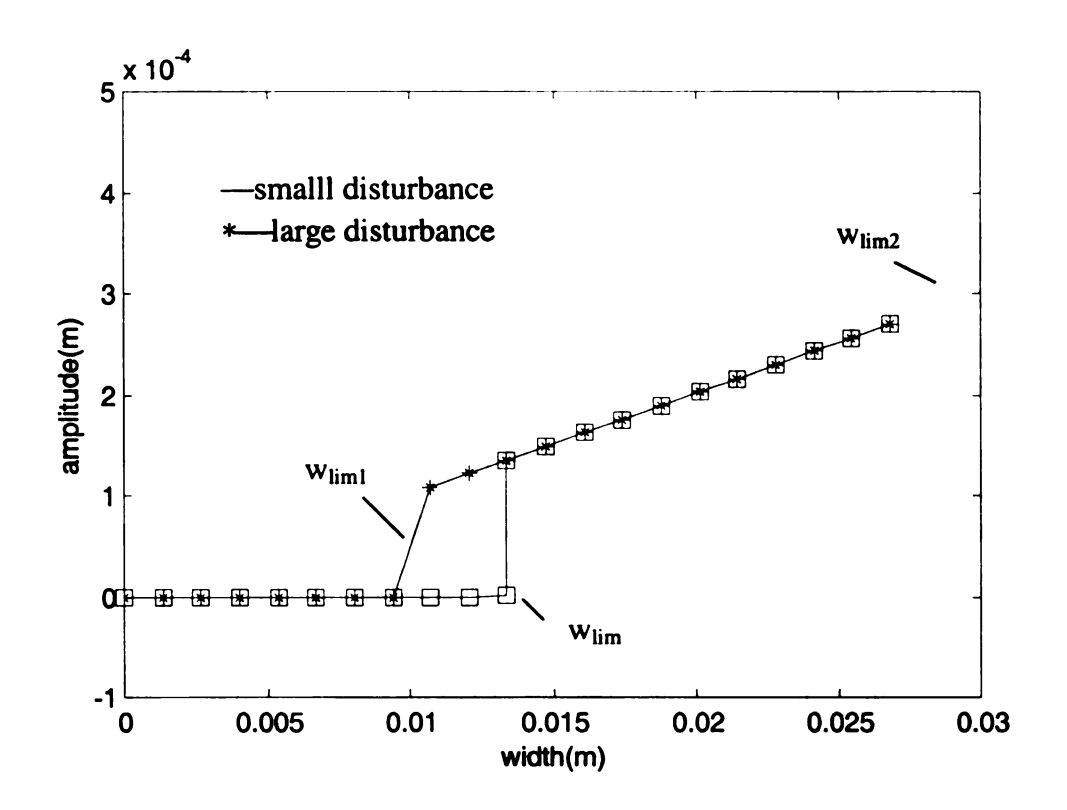


Figure 3.5 Simulations of subcritical period-doubling bifurcation diagram

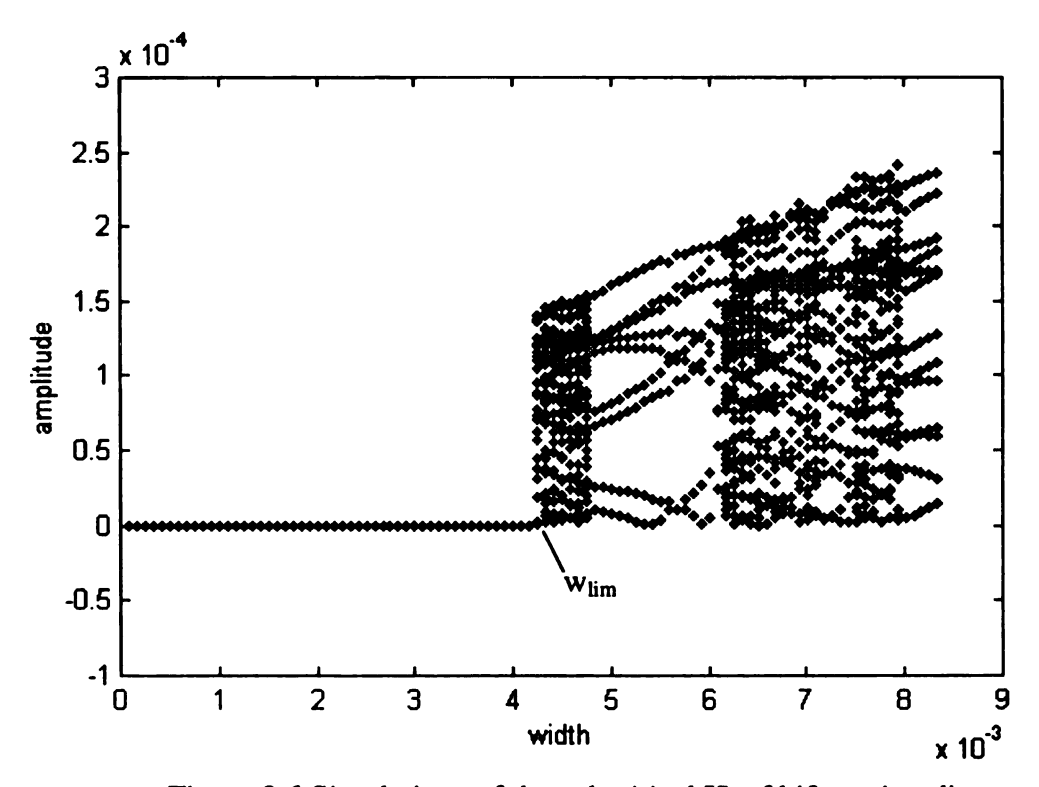


Figure 3.6 Simulations of the subcritical Hopf bifurcation diagram

Section 3.2: Experiments

In this paper, a nonlinear theory for predicting the stability of highly interrupted cutting is presented. The theory is based upon modeling the cutting as a kicked harmonic oscillator with delay which has been done by Davis et al. (1999a). On the contrary of the traditional regenerative chatter theory, the most important prediction of the new theory, from the practical perspective, is that the number of optimally stable speeds doubles as the ratio of the time spent cutting to not cutting decreases. Davis et al. (1999b) did some experiments to confirm this theoretical prediction.

The experiment below shows the new stable speeds with long-overhang end-milling in Figure 3.6. The ratio of the length and diameter of the cutter is 9:1, and the stability measurements were done for the tool for 25% and 5% immersion respectively. Notice the new stable region of spindle speeds between 18 krpm and 20 krpm for 5% immersion compared to 25% immersion.

Part of the stability charts from analytical prediction and from the experiments for the 9:1 tool is compared in Figure 3.7. It can be seen that the experiment agrees with the analytical prediction.

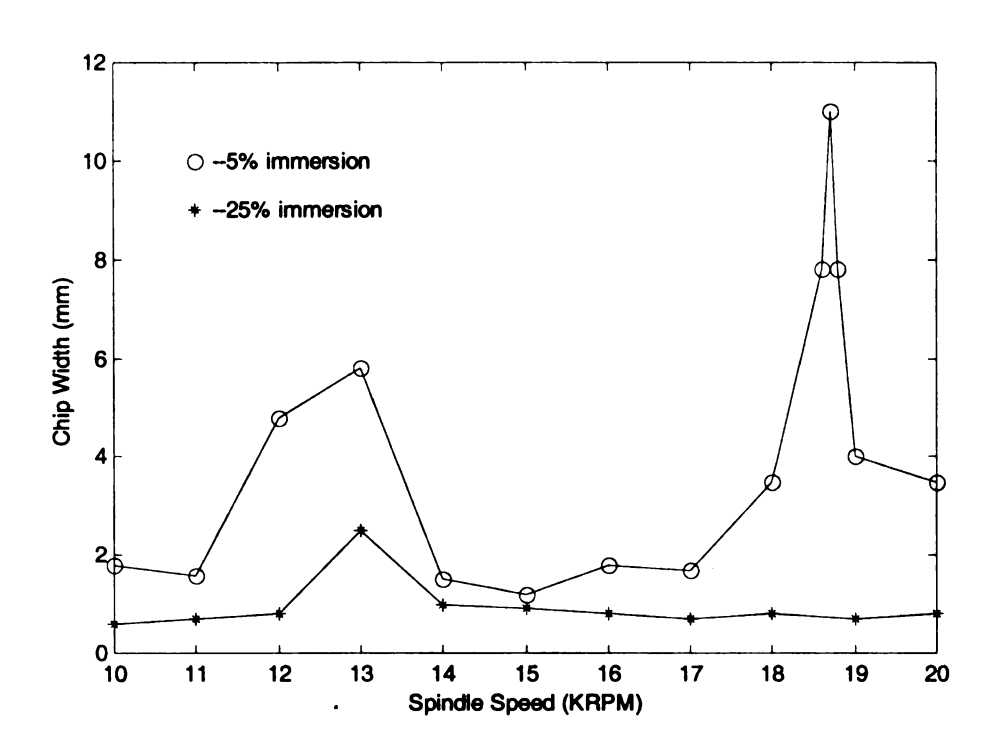


Figure 3.7 Comparison of stability charts from experiments of 5% immersion and 25% immersion end-milling. (Courtesy of M. A. Davis)

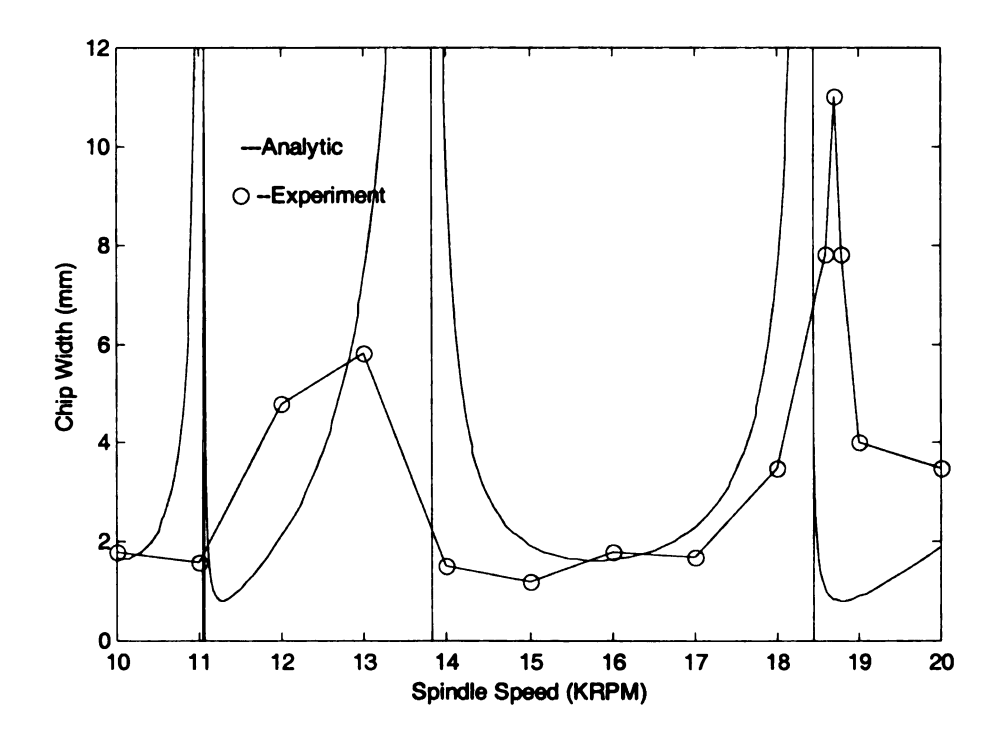


Figure 3.8 Comparison of stability charts from analytical prediction and experiments of 5% immersion end-milling. (Courtesy of M. A. Davis)

CHAPTER 4

CONCLUSIONS AND SUGGESTIONS FOR FUTURE WORK

Section 4.1: Conclusions

- An nonlinear model of interrupted machining is built. The machine tool structure
 is represented by an equivalent single degree of freedom system with the cutting
 forces by a digressive function (α) of chip thickness.
- 2. For highly interrupted machining, the system is simplified into an impact model and an analytic solution is obtained.
- The stability chart is analytically estimated. The number of stability lobes is doubled.
- 4. Besides Hopf bifurcation, Period-doubling bifurcation is also found in interrupted machining. Actually, the Hopf and period-doubling bifurcation occurs alternatively with the increase of spindle speed at certain cutting conditions.
- 5. Both Hopf bifurcation and period-doubling bifurcation are subcritical as $0<\alpha<1$. The effect of the value of α on the bifurcations is analyzed. When $0<\alpha<1$, the

- bifurcation is subcritical; when $\alpha=1$, the system becomes linear, and the chatter amplitude would be infinite; when $\alpha>1$, the bifurcation is supercritical.
- 6. The nonlinearity is also introduced by the vibrating tool leaving the workpiece frequently as the bifurcation occurs.
- Global bifurcations are analyzed. Period-two orbits and quasiperiodic orbits are predicted. Possible routes to chaos are discussed.
- 8. Numerical simulations verify the analytic results above. Hysteresis is found for subcritical bifurcations. The stable period-two orbit and quasiperiodic orbit are found and well agree with the analytic solution.

Section 4.2: Suggestions for future work

- 1. Experiments are in badly need to verify the analytic and numerical results. Some previous works (Shi, Tobias (1985), Nayfeh et al. (1997), etc.) have shown the subcritical instability and the hysteresis by experiments in the continuous cutting. Davies et al. (1999a, 1999b) have shown the doubling of the stability lobes with the linear model by the support of experiments, which proves both Hopf bifurcation and period-doubling bifurcation are possible in interrupted machining. But no experiments have been oriented to the subcritical/supercritical bifurcation in the interrupted machining.
- 2. Numerical simulations can be elaborated for low immersion milling to verify the analytic prediction. The immersion ratio (ρ) varies after bifurcation occurs, so it is better to use a shooting method to determine when the tool engages in cut, and

when it runs out of cut. Actually, further investigation on the low immersion milling inevitably results in a two-degree-of-freedom model and analytic solutions can no longer be obtained. Only numerical simulations are feasible.

3. Better mathematical model can be built with more considerations on the number of degree of freedom and nonlinearities on stiffness, damping. And the cutting force can be the nonlinear function of chip area or chip volume.

BIBLIOGRAPHY

Altintas, Y. and Budak, 1995, "Analytical prediction of stability lobes in milling", Annals of the CIRP, 44(1), pp357-362.

Arnold, R. N., 1946, "The mechanism of tool vibration in the cutting of steel", Proceedings of the Institution of Mechanical Engineers 154(4), pp. 261-284.

Davies, M. A., Dutterer, B., etc, 1998, "On the dynamics of high speed milling with long slender endmills", Annals of the CIRP, 47(1), pp55-60.

Davies, M. A., Pratt, J. R., Dutter, B., and Burns, T. J., 1999, "Interrupted machining— a doubling in the number of the stability lobes? Part 1: theoretical development", submitted to Journal of Manufacturing Science and Engineering.

Davies, M. A., Pratt, J. R., Dutter, B., and Burns, T. J., 1999, "Interrupted machining— a doubling in the number of the stability lobes? Part 2: numerical simulation and experiment", submitted to Journal of Manufacturing Science and Engineering.

Fishwick W., Tobias S.A., 1958, "Machine Tool Chatter, Effect of Flexibility in Machine and Foundation", Engineering, pp.568-572.

Grabec, I., 1988, "Chaotic dynamics of the cutting Process," Int. J. Mach. Tools Manuf., Vol. 28, pp. 19-32.

Guckenheimer, J., Holmes, P., 1983, "Nonlinear Oscillations, Dynamical Systems, and Bifurcations of Vector Fields", Springer-Verlag Inc.

Halley, J. E., Helvey, A. M., Smith, K. S., and Winfough, W. R., 1999, "The impact of high-speed machining on the design and fabrication of aircraft components", Proceedings of the 17th Biennial Conference on Mechanical Vibration and Noise, 1999 ASME Design and Technical Conference, Las Vegas, Nevada, September 12-16.

Hanna, N. H., Tobias, S. A., 1974, "A theory of nonlinear regenerative chatter", Journal of Engineering for Industry, Feb. pp247-255.

Hirsch, M. W., and Smale, S., 1974, Differential Equations, Dynamical Systems, and Linear Algebra, Academic Press, Inc., San Diego, California, USA.

Lin, J. S., and Weng, C. I., 1990, "A Nonlinear Dynamic Modle of Cutting," Int. J. Mach. Tools Manuf., Vol. 30, pp. 53-64.

Moon, F. C., 1994, Chaotic Dynamics and Fractals in Material Removal Processes, Non-linearity and Chaos in Engineering Dynamics, Thompson, J. M. T., And Bishop, S. R. eds., Wiley, New York.

Manneville, P. and Y. Pmeau, 1980, "Different ways to turbulence in dissipative dynamical systems", Physica D 1, 197, 201, 206, pp. 219-226.

Merrit, H. E., 1965, "Theory of Self-Excited Machine Tool Chatter- Contribution to Machine Tool Chatter Research – 1", Journal of Eng. For Industry, Trans. ASME, Series B, Vol. 87, No. 4, Nov. pp. 447-454.

Nayfeh, A. H. and Balachandran, B., 1995, Applied Nonlinear Dynamics, John Wiley and Sons, Inc.

Nayfeh, A. H., Chin, C.-M., Pratt, J., 1997, "Perturbation methods in nonlinear dynamics—applications to machining dynamics", Journal of Manufacturing Science and Engineering, Vol. 119, pp485-493.

Pmeau, Y., and Manneville, P., 1980, "Intermittent transition to trubulence in dissipative dynamical systems", Comm. Math. Phys. 74, 197, 201, 206, 298, pp.189-197.

Pratt, J. R., 1999, Personal Communications.

Shi, H. M., Tobias, S. A., 1984, "Theory of finite amplitude machine tool instability", Int. J. Mach. Tool Des. &. Res., Vol. 24, No. 1, pp45-69.

Shridar, E., Hohn, R. E. and Long, G. W., 1968, "A general formulation of the milling process equation", Journal of Engineering for Industry, 90, pp. 317.

Shridar, E., Hohn, R. E. and Long, G. W., 1968, "A stability algorithm for the general milling process", Journal of Engineering for Industry, 90, pp. 330.

Smith S., and Tlusty, J., 1991, "An overview of modeling and simulation of the milling process", ASME Journal of Engineering of Industry, 113, May, pp. 169-175.

Smith, S., Winfough, B. and Frost, J. 1994, "Automatic chatter avoidance using coincident stable speeds for competing modes", PED Vol. 68(2), Manufacturing Science and Engineering, ASME.

Smith, S. Jacobs, T. P. and Long, G. W., 1999, "The effect of drawbar force on metal removal rate in milling", Annals of the CIRP, 48(1), pp293-296.

Stephan, G. Kalmar-Nagy, T., 1997, "Nonlinear Regenerative machine tool vibrations", ASME Design Engineering Technical Conference, (DECT97/VIB-4021), pp1-11.

Taylor, F. W., 1907, "On the art of cutting metals", Transactions of the ASME, 28, pp. 31-35.

Tlusty, J., 1993, "High-speed machining", Annals of the CIRP, Vol. 42(2), pp733-728.

Tlusty, J. and Polocek, M., 1963, "The stability of the machine-tool against self-excited vibration in machining", Proceedings of the international research in production engineering, Pittsburgh, pp. 465, ASME New York.

Tlusty, J. and Ismail, F., 1983, "Special aspects of chatter in milling", ASME Journal of Vibration Stress and Reliability in Design, 105, pp. 24-32.

Tlusty, J., 1986, "The dynamics of high-speed milling", Journal of Engineering for Industry, 108, pp. 59-67.

Wiggins, S., 1990, "Introduction to applied nonlinear dynamical systems and chaos", Springer-Verlag Inc.

Zaslavsky, G. M. 1978, "The simplest case of a strange attractor", Phys. Lett. A, 69(3), pp. 145-147.

Zaslavsky, G. M., Sagdeev, R. Z., 1991, Weak Chaos and Quasi-reqular Patterns, Cambridge University Press, Cambridge, England.

Zhao, M. X., Balachandran, B., Davies M. A., Pratt, J. R., 1999, "Dynamics and stability of partial immersion milling operations", ASME Design Engineering Technical Conference, (DECT99/VIB-8058), pp1-6.

